



**1 Assessing the drought resilience of different land management scenarios using a tracer-aided
2 ecohydrological model with variable root uptake distributions**

3 Cong Jiang¹, Doerthe Tetzlaff^{1,2,3}, Songjun Wu¹, Christian Birkel^{1,4}, Hjalmar Laudon⁵, Chris Soulsby^{1,3,5,6}

4 ¹ Leibniz-Institute of Freshwater Ecology and Inland Fisheries (IGB), Department of Ecohydrology and
5 Biogeochemistry, Berlin, Germany

6 ² Department of Geography, Humboldt University Berlin, Berlin, Germany

7 ³ Northern Rivers Institute, University of Aberdeen, Aberdeen, UK

8 ⁴ Department of Geography, University of Costa Rica, San Pedro, Costa Rica

9 ⁵ Department of Forest Ecology and Management, Swedish University of Agricultural Science (SLU), Sweden

10 ⁶ Chair of Water Resources Management and Modeling of Hydrosystems, Technical University Berlin, Berlin,
11 Germany

12 *Correspondence to:* Cong Jiang (cong.jiang@igb-berlin.de)

13 **Abstract.** Land use strongly influences water partitioning, availability, and ecohydrological resilience in drought-
14 sensitive regions. Forest management plays a critical role through its effects on water use, which depends on
15 species composition, stand density, rooting depth, canopy structure, and age. However, the ecohydrological
16 consequences of different forest management strategies—particularly in terms of blue and green water fluxes—
17 remain poorly quantified for land use planning. This study conducted a series of modelling experiments using the
18 tracer-aided conceptual ecohydrological model EcoPlot-iso as a decision-support tool. We investigated how
19 variations in forest type (e.g., broadleaf vs. conifer), density, and root distribution influence water partitioning and
20 ecohydrological resilience under different wetness conditions in the drought-sensitive lowland Demnitzer
21 Millcreek catchment (DMC), northeastern Germany. Baseline simulations (2000–2024) across several land use
22 types were used to develop a reference forest for comparison with alternative forest management scenarios. A key
23 innovation in this version of EcoPlot-iso was the integration of a depth-dependent root water uptake function,
24 allowing simulation of transpiration across forests with different rooting distribution, stand ages, and species
25 compositions. The model was calibrated and validated using seven years of soil moisture and three years of soil
26 water isotope ($\delta^2\text{H}$) data through a multi-criteria approach. Results showed that, on average, evapotranspiration
27 was 8% higher under conifers than broadleaf forests, and 12% higher than agroforestry. Agroforestry, in contrast,
28 provided the highest groundwater recharge—11% and 4% more than conifers and broadleaf forests, respectively.
29 Significant differences in water partitioning between dry and wet years were observed across management
30 scenarios. Our findings highlight the potential of agroforestry, such as crop–tree mixtures, to mitigate drought
31 impacts. The modelling framework provides a means to quantify and visualise the effects of land use change on
32 water availability, supporting more informed decision-making for resilient land and water management.

33 **1 Introduction**

34 Land use plays a crucial role in regulating water, carbon, energy, and nutrient cycles by mediating ecohydrological
35 fluxes and soil water storage dynamics which link interactions between the atmosphere, soils, vegetation and
36 biogeochemical processes (Mahmood et al., 2014; Pielke et al., 2011; Smith et al., 2021; Sterling et al., 2013).
37 Among the different types of land cover, forests are particularly important elements of the land use mosaic,
38 providing a range of ecosystem services, including enhancing infiltration, stabilizing soils, storing carbon,
39 supplying timber and fuelwood, as well as buffering extreme climate events (Bonan, 2008). However, there are



40 clear trade-offs, as forests and trees also tend to use more water than contrasting land uses (Bosch & Hewlett,
41 1982; Calder, 1998). This is because their high Leaf Area Index (LAI) and canopy storage capacities often result
42 in great interception losses and canopy evaporation, while their deep and dense rooting networks can sustain
43 transpiration when top soils dry out (Wang-Erlandsson et al., 2014). Consequently, forest management decisions,
44 (e.g., afforestation, thinning, species selection etc.) can significantly affect water yield, the partitioning into blue
45 (runoff, groundwater recharge) and green (evapotranspiration) water fluxes, and overall drought resilience
46 (Falkenmark & Rockström, 2006; Neill et al., 2021).

47 Sustainable land management also requires consideration of sensitivity to climate change, which is altering
48 hydroclimatic regimes by shifting precipitation patterns, intensifying drought frequency and duration in many
49 areas (Huntington, 2006; Trenberth, 2011). These changes can increase atmospheric demand and evaporative
50 losses, reducing groundwater recharge and surface water availability, and thus exacerbating water scarcity in many
51 regions (Ault, 2020; Yuan et al., 2023). As land use practices—particularly forest management—strongly
52 influence water partitioning, understanding their impacts under changing hydroclimatic conditions is essential for
53 maintaining resilient water and land systems, especially in drought-prone areas.

54 The understandings on how land use change affects runoff generation, soil moisture storage and
55 evapotranspiration dynamics have been gradually developed through decades of research, including long-term
56 experimental watershed studies such as paired catchment experiments on water yield (Bosch & Hewlett, 1982;
57 Brown et al., 2005, 2013; Hibbert, 1967). However, quantifying the impact of forest management on water
58 partitioning remains challenging (Guswa et al., 2020). This is due to the complex interplay of climate conditions,
59 soil properties, vegetation type, and topography, and the difficulty in distinguishing individual ET components
60 (Kool et al., 2014; Smith et al., 2021; Zhang et al., 2001). These challenges are further compounded by scarce
61 long-term observational data for forest ecosystems, which are essential given their slow dynamics and lengthy
62 growth cycles (Tetzlaff et al., 2017). In forest ecosystems, ET is particularly difficult to simulate due to complex
63 interactions among canopy structure, stomatal behavior, and root water uptake (Tague & Band, 2004). Although
64 many ecohydrological models include some form of root water uptake conceptualization (e.g., mHM, EcH2O-
65 iso), the dynamic and species-specific nature of root distribution and function is usually inadequately represented.
66 This limits the ability of models to fully capture the effects of forest age, species composition, and management
67 practices on transpiration and soil–plant water fluxes (Dubbart et al., 2023; Kumar et al., 2015). Recent isotope-
68 based studies (e.g., Knighton et al. (2020)) have advanced understanding of root water uptake (RWU) dynamics,
69 yet key knowledge gaps remain, including spatiotemporal variability and species-specific uptake strategies
70 (Knighton et al., 2024). Moreover, traditional hydrological models often struggle to separate evaporation and
71 transpiration, limiting their ability to accurately simulate the long-term effects of land management on water
72 partitioning, vegetation dynamics and soil water storage (Birkel et al., 2025) Additionally, while complex climate
73 and land surface models offer detailed representations by coupling multiple biophysical processes, they often
74 require extensive computational resources and dense parameterization resulting in high uncertainty (Ricci et al.,
75 2020). Despite their complexity, many sophisticated models are difficult to effectively calibrate, leading to higher
76 parametric uncertainty—particularly in data-scarce regions (e.g., Fatichi et al. 2012; Tague & Band 2004). As a
77 result, these models may have limited capacity to accurately represent the long-term water partitioning dynamics
78 and subtle ecohydrological feedbacks associated with forest structure, root water uptake, and land management.



79 This highlights the need for complementary simpler, systematic, long-term modeling approaches that integrate
80 realistic forest management scenarios to better represent water partitioning and ecohydrological resilience.

81 Tracer-based ecohydrological modelling offers a promising approach to address these challenges by improving
82 the characterization of water movement, mixing and storage dynamics under different land cover types (Landgraf
83 et al., 2023; Luo et al., 2024). Stable water isotopes serve as natural tracers and offer unique isotopic fingerprints
84 that can differentiate between evaporation and transpiration. This distinction is essential for refining our
85 understanding of ecosystem water use and for better quantifying the timing and magnitude of water fluxes and
86 storage. These models, which integrate climatic inputs, vegetation, water and soil dynamics, can facilitate more
87 robust predictions of ecohydrological responses to land use change and management. However, while complex
88 process-based, tracer-aided ecohydrological models, e.g. EcH2O-iso (Kuppel et al., 2018; Wu et al., 2023),
89 incorporate vegetation dynamic modules that enhance process representation, they tend to be highly parameterized,
90 computationally demanding and require extensive input data (Douinot et al., 2019). In contrast, tracer-aided model
91 of more intermediate complexity, such as the conceptual, tracer-aided model EcoPlot-iso (Landgraf et al., 2023;
92 Stevenson et al., 2023) provides a simplified modelling tool that has been shown to provide a robust process-
93 based framework quantifying the effects of land use on water partitioning (Birkel et al., 2024, 2025).

94 In this study, we apply the tracer-aided conceptual model EcoPlot-iso to assess how land use – specifically forest
95 management strategies - influences water partitioning and soil moisture storage in the drought-sensitive, lowland
96 Demnitzer Millcreek catchment, NE Germany. The catchment is typical of large areas in central Europe where
97 freely draining, sandy soils combine with a relatively dry and warm climate to limit water availability. To improve
98 the quantification of transpiration, we introduce a novel development in EcoPlot-iso by integrating a depth-
99 dependent root water withdrawal function into the transpiration equation. The model is dual-calibrated and
100 validated using seven years of soil moisture data and three years of soil water isotope data. A series of generic
101 forest management scenarios—varying in forest density, canopy structure (deciduous, coniferous, agroforestry),
102 and rooting characteristics—are developed to explore their impacts on vertical water fluxes and ecohydrological
103 resilience.

104 This study aims to answer the following research questions:

- 105 ➤ How does vegetation cover influence water use and partitioning under varying wetness conditions
106 in a drought-sensitive, lowland catchment?
- 107 ➤ What are the implications of alternative generic forest management scenarios for water availability
108 and overall ecohydrological resilience?
- 109 ➤ How can we optimize the land management strategies to mitigate drought impacts and enhance
110 ecohydrological resilience in the face of climate change?

111 2 Study area

112 2.1 Demnitzer Millcreek catchment (DMC)

113 The Demnitzer Millcreek catchment (DMC) is a 66 km² lowland basin (30–90 m elevation) in the State of
114 Brandenburg, Germany, approximately 55 km east of Berlin (52°23' N, 14°15' E) (Figure 1). Located in the



115 Northern European Plain, it is part of a drought-sensitive region that provides many essential ecosystem services,
116 including agriculture, timber production, and water supply.

117 The DMC landscape is dominated by non-irrigated farmland, mostly arable crops and some grazing on more
118 water-retentive soils brown and gley soils respectively which cover 60% of the catchment in the (Fig. 1a and b).
119 Forests cover 36% of the catchment, and include coniferous, broadleaf, and mixed stands. Small urban settlements
120 (2%) are scattered throughout the catchment, with wetlands on peat soils primarily found along streams in the
121 central part of the catchment. The climate is temperate with warm summers, with a mean annual temperature of
122 9.6°C and average precipitation of approximately 558 mm, based on weather station data from 2000 to 2024 (see
123 Table 2). Potential evapotranspiration (PET) ranges from 584 to 789 mm per year from 2000 to 2024, based on
124 calculations from this study (see Table 2). Interannual variability in precipitation, including the identification of
125 dry and wet years, is shown in Figure S3, which highlights deviations from the long-term mean and helps
126 contextualize recent drought impacts. Rainfall peaks in summer, accompanied by intense convective storms;
127 however, surface runoff is rare, as the soils are highly permeable and dry in the growing season. Consequently,
128 the catchment is primarily groundwater-dominated with winter high flows and often dries in the summer (Smith
129 et al., 2021). The geology consists mainly of glacial and fluvial deposits and base moraines, while the dominant
130 soil types include poorly drained silty gley brown earth and well-drained podzolic brown earth soils (Figure 1b).

131 The DMC has a long history of human influence, with significant land use changes affecting its hydrology. In the
132 18th Century, artificial drainage channels were constructed to convert wetlands into agricultural land. Since the
133 1990s, efforts in wetland restoration and wildlife recolonization (e.g., beaver recovery) have aimed to enhance
134 water retention in the landscape. Long-term hydrological and isotopic monitoring (Gelbrecht et al., 1996, 2005;
135 Smith et al., 2020; Wu et al., 2021) has provided valuable insights into the impacts of agriculture and land use
136 management on water quality, ecohydrological partitioning and soil water storage. The 2018 European drought
137 and subsequent prolonged dry periods have exacerbated water scarcity and ecosystem vulnerability (Kleine et al.,
138 2021). In response, some land owners have explored agroforestry and other adaptive forest and tree management
139 strategies to improve water retention and landscape resilience (Luo et al., 2024). Agroforestry represents a
140 transitional system blending low density tree cultivation and with agriculture; either in terms of grazing the
141 understory vegetation or crops (Landgraf et al., 2022; Quandt et al., 2023). Such systems are characterized by
142 minimal canopy cover and no artificial irrigation, though mulching is often used to enhance soil moisture storage.
143 Such systems typically involve rows of small deciduous trees or shrubs (≤ 2 m in height), spaced 2–3 m apart,
144 interplanted with rainfed legumes (Landgraf et al., 2023). Given the long-term monitoring record and ongoing
145 land use change, DMC serves as a useful site for assessing the impacts of changing forest management on water
146 partitioning, soil moisture and ecohydrological resilience under different wetness conditions.

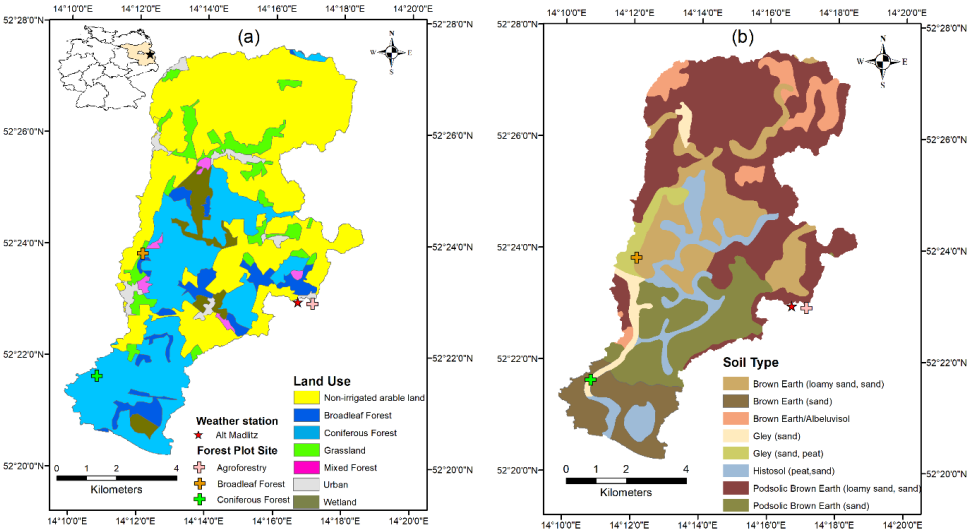


Figure 1. Location, land use (a) and soil type (b) map of the Demnitzer Millcreek catchment, showing the current distribution of broadleaf forests, conifer forests, agroforestry, cropland, and grassland.

2.2 Forest Plot Site

To investigate the effects of forest management scenarios on water partitioning and ecohydrological resilience, a monitoring predominantly broadleaf forest plot site was selected within the drought-sensitive DMC in the NE Germany. This plot represents a key forest type central to the modelling experiments: a relatively mature (~60 years old) broadleaf forest system. Moreover, it is formed on the extensive freely draining sandy brown soils that are particularly drought sensitive in DMC due to their poor water retention characteristics. The location is shown in Figure 1, and site characteristics are described below with more details available in Kleine et al. (2021) and Landgraf et al. (2023).

Specifically, the broadleaf forest site is dominated by mature European oak (*Quercus robur*) with a few Scots pine (*Pinus sylvestris*) present within the plot. Additional species including Norway maple (*Acer platanoides*), elm (*Ulmus* spp.), and hazel (*Corylus avellana*) are found within 10 m of the plot boundary. The soil is a freely draining Lamellie Brunic Arenosol (Humic), characterized by loamy sand to sand textures. This corresponds to a typical brown earth in regional classification systems.

Table 1. Summary observed soil type and soil moisture at three forest sites.

Site	Soil Type	Texture	Layer	Soil Moisture (mm)			
				Max	Min	Mean	SD
Broadleaf forest	Brown Earth	Loamy sand/sand	0 to 10 cm	26.28	3.50	13.67	6.30
			10 to 30 cm	56.19	6.86	24.68	11.70
			30 to 100 cm	147.51	25.83	71.71	33.50
			10 to 30 cm	53.35	7.15	29.75	13.49
			30 to 100 cm	223.62	86.83	163.41	41.98

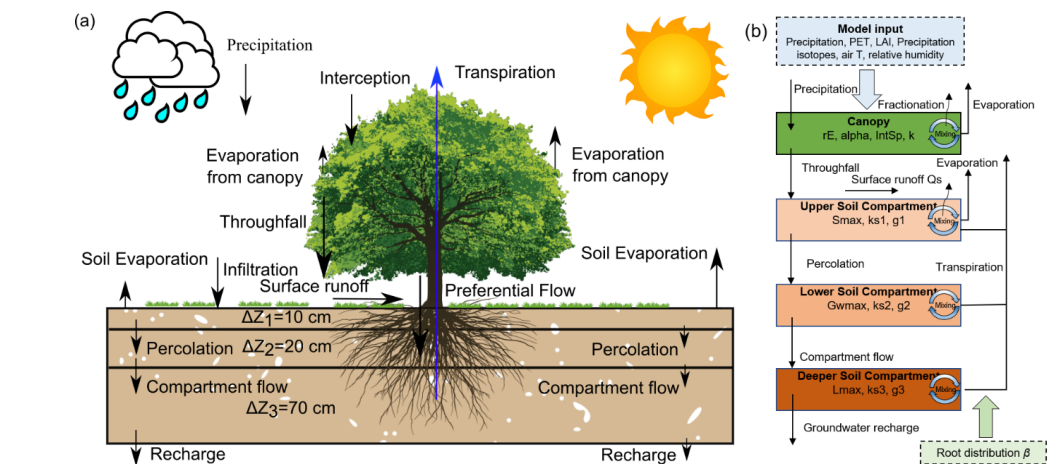


164 **3 Method and Data**

165 **3.1 Model Framework and Structure**

166 This study employs the EcoPlot-iso model, a tracer-aided ecohydrological modelling framework designed to
167 simulate key ecohydrological and isotopic transformations that characterise water partitioning at the plot scale
168 (Birkel et al., 2024; Landgraf et al., 2023; Stevenson et al., 2023). EcoPlot-iso is a process-based conceptual model
169 that simulates key ecohydrological fluxes, including interception, throughfall, infiltration, preferential flow,
170 surface runoff, percolation, and groundwater recharge, as well as evapotranspiration components such as canopy
171 evaporation, soil evaporation, and transpiration (Figure 2a). These processes are represented within a vertical
172 structure comprising a single canopy layer and three soil layers (0–10 cm, 10–30 cm, and 30–100 cm) (Figure 2b).
173 Recently, the isotope tracking module was further developed to include fractionation and mixing processes,
174 allowing EcoPlot-iso to differentiate evaporation from transpiration and improve water flux estimates. The
175 required input variables (Table 2) include meteorological data such as precipitation, potential evapotranspiration
176 (PET), air temperature, and relative humidity, along with isotopic data (precipitation isotope) and vegetation-
177 related parameters (leaf area index, LAI).

178 EcoPlot-iso has been applied in diverse climatic and hydrological settings, including a one-year simulation in
179 Scotland (Stevenson et al., 2023), a one-year simulation at the Demnitzer Millcreek (DMC) site in the Northern
180 European Plain (Landgraf et al., 2023), and a four-year simulation in the humid tropics of Costa Rica (Birkel et
181 al., 2024). Building on these applications, this study employs EcoPlot-iso for a long-term tracer-aided
182 ecohydrological simulation to assess the effects of different forest management scenarios on water partitioning
183 and ecohydrological resilience.



184
185 **Figure 2.** (a) Schematic representation of the ecohydrological fluxes and water partitioning in the EcoPlot-iso
186 model illustrating major water fluxes and storage components; (b) Conceptual framework and key parameters of
187 the EcoPlot-iso model (Landgraf et al., 2023; Stevenson et al., 2023), highlighting the key ecohydrological
188 processes simulated in this study.



189 3.2 Model Adaptations: Integrating Root Distribution into the Transpiration Equation

190 Although root water uptake plays a critical role in soil–plant–atmosphere interactions, it was not explicitly
191 represented in EcoPlot-iso (Stevenson et al., 2023) This study introduces a novel depth-dependent root uptake
192 function to improve the model’s simulation of transpiration and water partitioning across different root
193 distributions. This adaptation enables the model to account for variations in rooting depth and water uptake
194 efficiency across land use types—such as young and mature forests or contrasting vegetation covers—that affect
195 soil water extraction. Specifically, a new transpiration equation was implemented to calculate root water uptake
196 across three soil compartments—shallow, middle, and deep—by incorporating depth-specific uptake efficiency:

$$197 \quad T_{p1} = r_{L1} * (T_p - E_i) * \left(\frac{STO}{S_{max}} \right) \quad (1)$$

$$198 \quad T_{p2} = r_{L2} * (T_p - E_i - T_{p1}) * \left(\frac{GW}{GW_{max}} \right) \quad (2)$$

$$199 \quad T_{p3} = r_{L3} * (T_p - E_i - T_{p1} - T_{p2}) * \left(\frac{SDeep}{SDeep_{max}} \right) \quad (3)$$

200 where T_{p1} , T_{p2} , T_{p3} represent the transpiration from the upper, lower, and deeper soil compartments, respectively.
201 E_i denotes the canopy evaporation. STO , GW , $SDeep$ represent the water storage in the upper, lower, and deeper
202 soil compartments. S_{max} , GW_{max} , L_{max} are the maximum water storage capacities of these compartments. r_{L1} , r_{L2}
203 and r_{L3} represent the root water withdrawal efficiency in the upper, lower, and deeper soil compartments,
204 respectively.

205 To explicitly link root water uptake to soil moisture availability and transpiration demand, an efficiency factor $r(z)$
206 was introduced. The exponential root water withdrawal efficiency function is defined as:

$$207 \quad r(z) = e^{-\beta z} \quad (4)$$

208 where $r(z)$ represents the capacity of roots to extract water at depth z , and β is the decay rate, which determines
209 how quickly root activity decreases with increasing depth. A higher β value concentrates root activity near the
210 surface, while lower β values allow for deeper water uptake (see Supplement Figure S1).

211 3.3 Model Setup and Input and Observation Data

212 The EcoPlot-iso model was applied to DMC across four sites with different dominant land use: broadleaf forest,
213 cropland, agroforestry, and grassland over a 25-year period (2000–2024) at daily timesteps. Soil moisture
214 initialization was based on observed data, and a one-year spin-up period was included before each simulation to
215 stabilize initial conditions. The input datasets required for the model—climate, vegetation, soil moisture, and
216 isotope data—are summarized in Table 2. Climate variables, including precipitation, temperature, wind speed,
217 and relative humidity, were primarily obtained from the Müncheberg weather station (DWD, German Weather
218 Service, ~20 km from DMC). Potential Evapotranspiration (PET) was calculated using the FAO Penman-
219 Monteith equation, while net radiation was derived from ERA5 reanalysis data (Hersbach et al., 2020). The Leaf



Area Index (LAI) was obtained from the MODIS 8-day resolution dataset and interpolated to daily timesteps. To improve accuracy and reduce data noise, the MODIS LAI was further adjusted using in-situ LAI measurements (maximum and minimum values), following Smith et al. 2021 and Wu et al. (2023). The complete set of time series input data used to drive the EcoPlot-iso simulations in the Demnitzer MillCreek Catchment for 2000–2004—including daily precipitation, precipitation isotopes ($\delta^2\text{H}$), air temperature, relative humidity, Leaf Area Index (LAI), and potential evapotranspiration (PET)—is presented in Figure S2 of the Supplementary Material.

Surface soil moisture (0–10 cm) was measured using a handheld soil moisture device on a monthly basis during two periods of more detailed observations in 2018–2019 and in 2021. For subsurface soil moisture, permanently installed soil moisture probes (two replicates at each depth) were used to continuously monitor Volumetric Water Content (VWC) at 15-minute intervals at four sites (Figure 1). To facilitate data processing and consistency, all soil moisture datasets were aggregated into daily mean values, resulting in one VWC value per site and soil depth. A summary of the measurement devices, depth intervals, and aggregation methods is summarized in Table S1. Daily precipitation samples for stable isotope analysis from June 2018 onward were collected at the Hasenfelde AWS, and earlier data were obtained from the Berlin weather station. Soil water isotopes were sampled from bulk soil at the four plot sites at five depths (0–5, 5–10, 10–20, 20–30, and 30–50 cm) every 3–4 weeks during the growing season. The isotope data were aggregated according to the thickness of the corresponding model soil compartments. All isotope values are reported relative to Vienna Standard Mean Ocean Water (VSMOW). Further details on site instrumentation and data collection are described in Landgraf et al. (2022).

Table 2. Summary of the used climate, vegetation, soil moisture, and isotope data

Data	Unit	Period	Timestep	Acquisition
Climate data				
Precipitation	mm/d	2000-2024	Daily	Muencheberg weather station (52.52°, 14.12 °)
Temperature	°C			
Windspeed	m/s			
Relative humidity	%			
Net shortwave radiation	W/m²		Hourly	ERA5
Net longwave radiation				
Potential evapotranspiration	mm/d	Daily	FAO Penman-Monteith equation	
Vegetation data				
Leaf area index	-	2000-2024	8-days	MODIS at broadleaf forest, coniferous, and agroforestry sites
Soil data				
Soil moisture	%	2018-2024	Daily	broadleaf forest, cropland, agroforestry, and grassland sites
Isotope data				
Precipitation isotope δ²H	‰	2000-2024	Daily	Hasenfelde (52.41°N, 14.19°E), weather station in Berlin
Soil water isotope		2018-2019, 2021	Daily	Manually at broadleaf forest, cropland, agroforestrv. and grassland sites



240 3.4 Model Calibration and Validation

241 The EcoPlot-iso model was calibrated using the Monte Carlo method and a multi-criteria approach based on soil
242 moisture and soil water isotope data for each site. For each model run, a total of 100,000 parameter sets were
243 generated using the Latin Hypercube Sampling (LHS) within a Monte Carlo framework (McKay et al., 1979) to
244 broadly sample the parameter space and capture a wide range of plausible model behaviors. The initial parameter
245 ranges, representing the widest physically feasible values for the site, were determined based on a literature review
246 and site-specific knowledge, with identical constraints applied across all vegetation types.

247 Model performance was evaluated using the modified Kling-Gupta Efficiency (*mKGE*) (Kling et al., 2012),
248 optimizing the averaged *mKGE* for soil moisture (*mKGE_{sm}*) and soil water isotopes (*mKGE_{iso}*) across the three
249 soil depth layers (*i*) to ensure robust parameter selection (Eq. 5). Calibration followed a two-step refinement
250 process. In the first step, based on the initial parameter ranges, the top 60th percentile of best-performing
251 simulations—ranked by average *mKGE*—along with their corresponding calibrated parameter sets, were retained.
252 In the second step, the model was re-run using the retained parameter space, and the 100 best simulations were
253 selected from the top 60th percentile to ensure optimal parameter selection. The model parameters, their initial
254 ranges, and the refined ranges for each of land use are summarized in Table S2 in the Supplement.

$$255 \quad mKGE = \frac{\sum_i^3 mKGE_{sm} + \sum_i^3 mKGE_{iso}}{6} \quad (5)$$

256 3.5 Development and Application of a Generic Forest Management Scenario Framework

257 To assess the general impacts of different forest management strategies on water partitioning and ecohydrological
258 resilience, we developed a framework for quantifying generic forest management scenarios based on simulations
259 at the broadleaved forest site at DMC. Baseline simulations (2000–2024) were established using EcoPlot-iso at
260 the broadleaf forest site.

261 From this baseline calibration, we retained the top 100 best-performing simulations—ranked by average modified
262 Kling-Gupta Efficiency (*mKGE*)—and their corresponding parameter sets. These calibrated parameter sets were
263 then used for scenario testing to ensure robust model performance across all simulations. To isolate the effects of
264 forest characteristics and management, all scenario simulations were driven using the same climate input data and
265 precipitation isotope time series as the baseline, along with consistent forcing data for potential evapotranspiration.
266 Additionally, site-specific Leaf Area Index (LAI) data were adjusted for the three forest types: broadleaf,
267 coniferous, and agroforestry, which were derived from 8-day MODIS remote sensing products (2000–2024)
268 (Table 2 and Figure S2d).

269 The scenario framework varied three key dimensions of forest management:

- 270 a) Forest density was varied by multiplying the reference Leaf Area Index (LAI) by a scaling factor ranging
271 from 0.2 to 1.8. Higher forest density was represented by scaling factors >1.0, indicating denser canopy
272 cover, while lower forest density corresponded to factors <1.0, reflecting more open canopy conditions.
- 273 b) Species composition was varied by implementing three canopy types—broadleaf, conifer, and
274 agroforestry—each assigned type-specific LAI values derived from MODIS data corrected using site
275 data at DMC (see Section 3.3) to reflect differences in forest structure and function.



276 c) Root water uptake efficiency was varied by parameterizing β values ranging from 0 to 2.0 to represent
277 vertical root distribution. Lower β values indicated deeper rooting systems (e.g., older or deep-rooted
278 species), while higher values represented shallower rooting systems (see Fig. S1).

279 This generic and scalable framework enables systematic simulation of long-term forest management impacts on
280 water partitioning, soil moisture dynamics, and ecohydrological resilience under consistent climatic conditions.
281 Although EcoPlot-iso was originally developed for plot-scale applications, it is applied here to represent
282 ecohydrological fluxes in a range of well-characterized sites within the DMC region. The model employs a one-
283 dimensional approach that does not explicitly account for lateral fluxes; however, this simplification is intentional.
284 It enables clearer interpretation of process-level dynamics under contrasting vegetation and climate conditions,
285 making it suitable for general scenario analysis. This assumption is especially justified in the DMC catchment,
286 which is characterized by flat, lowland topography and is predominantly governed by vertical hydrological fluxes
287 (Kleine et al., 2021; Smith et al., 2020).

288 The aim was not to reproduce exact spatial patterns, but to develop a generalizable understanding of how forest
289 structure influences vertical water fluxes and soil moisture. The framework thus serves as a practical tool for
290 assessing broad ecohydrological responses to forest management. Ultimately, the goal was to inform stakeholders
291 of the potential impacts of changes in canopy structure and forest age on long-term water availability and
292 ecohydrological resilience in drought-sensitive lowland catchments.

293 4 Results

294 4.1 Dynamics of Soil Moisture and Soil Water Isotopes at the Broadleaf Forest Site

295 Figure 3 shows the 25-year baseline simulations of soil moisture and soil water isotopes at the broadleaf forest
296 site. In general, the model effectively captures the magnitude, frequency, extremes, and timing of soil moisture
297 dynamics. Model results show surface soil moisture shows higher variability than deeper layers. Based on the
298 Kling-Gupta Efficiency (KGE), soil moisture simulations appear to perform better in the deep layer than in the
299 shallow and lower layers, though this may partly reflect the more limited variance in deeper soil moisture. In
300 addition, the model slightly overestimates low soil moisture in the deeper layers during wet summers (e.g., 2023,
301 2024) and underestimates soil moisture during dry winters (e.g., 2021 and 2022). Furthermore, soil water isotope
302 simulations perform well, with better performance in the intermediate layer than in surface and deeper layers in
303 terms of KGE. The uncertainty range of soil water isotope simulations is narrower than that of soil moisture,
304 indicating lower uncertainty in the isotope predictions.

305 Table 3 shows the Kling-Gupta Efficiency (KGE) values for soil moisture and soil water isotopes across different
306 land use plots. In all other cases the KGEs for soil moisture are similar to the broadleaved plot, and soil water
307 isotopes are reasonably reproduced, indicating the model's robustness and transferability. These results provide
308 strong support for the appropriateness of applying EcoPlot-iso to assess the impacts of alternative forest
309 management scenarios in subsequent analyses.

310

311



Table 3. Kling-Gupta Efficiency (KGE) values for soil moisture and $\delta^2\text{H}$, based on observed values compared to the mean simulated values.

Forest sites	Soil moisture			Soil water isotope $\delta^2\text{H}$		
	Upper soil compartment	Lower soil compartment	Deep soil compartment	Upper soil compartment	Lower soil compartment	Deep soil compartment
Broadleaf Forest	0.60	0.72	0.84	0.58	0.74	0.64
Agroforestry	0.72	0.76	0.78	0.81	0.84	0.78
Grassland	0.87	0.67	0.71	0.72	0.76	0.60
Cropland	0.53	0.54	0.71	0.82	0.84	0.28

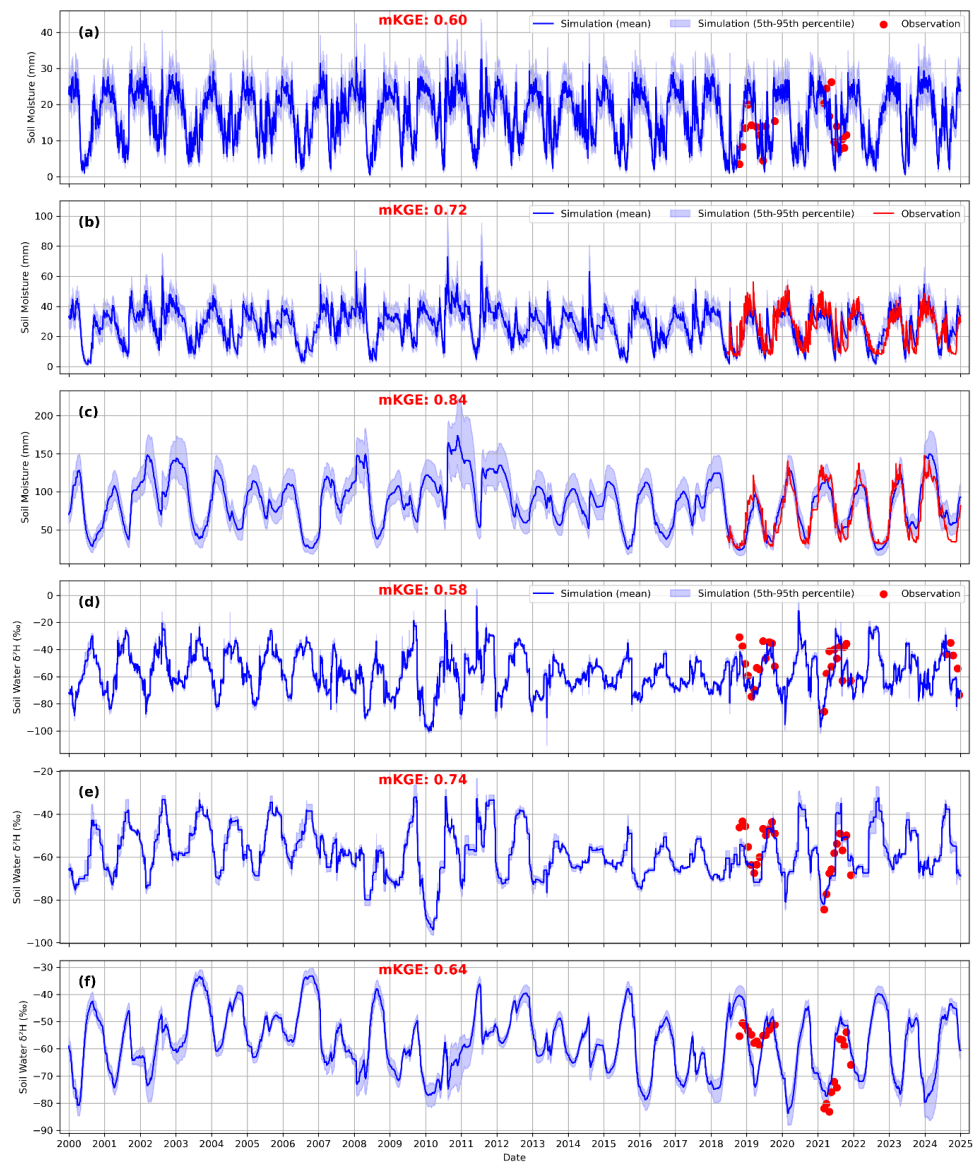
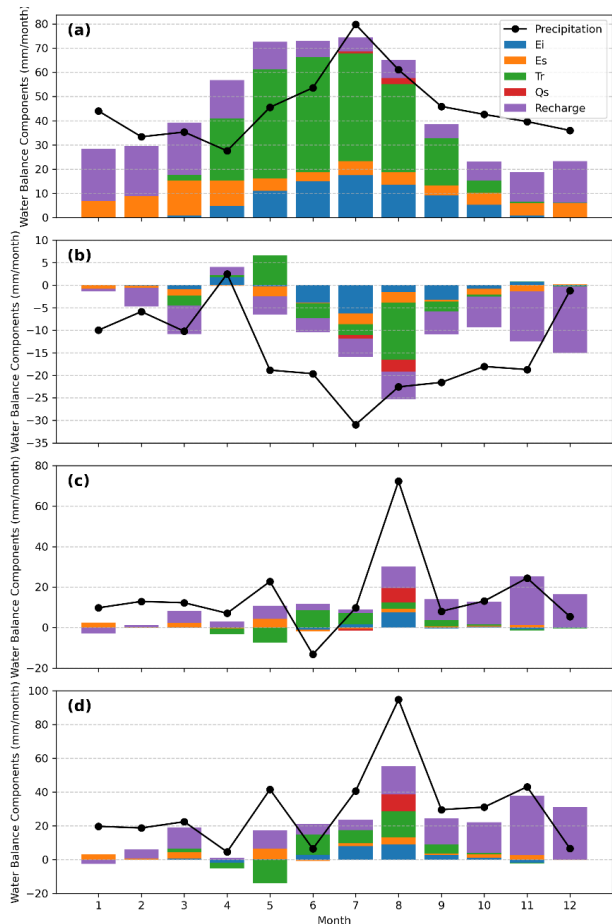


Figure 3. Long-term (2000–2024) simulations of soil moisture and soil water isotope ($\delta^2\text{H}$) at three different depths using EcoPlot-iso at a broadleaf forest site in the Demnitzer Millcreek catchment. (a–c) Simulated (mean \pm 5th–95th percentile) and observed soil moisture at surface (0–10 cm), lower (20–30 cm), and deeper (30–100 cm) layers. (d–f) Simulated (mean \pm 5th–95th percentile) and observed soil water isotopic composition ($\delta^2\text{H}$) at corresponding depths. The blue line represents the mean value of the 100 best simulations, while the shaded area indicates the range between the 5th and 95th percentiles of these simulations. The red points and red line represent observed values. Kling-Gupta Efficiency (KGE) values for each simulation are indicated in the respective panels.



326 **4.2 Water Balance Components Under Different Wetness Conditions**

327 Figure 4 presents the mean monthly water balance components and their changes between dry and wet years for
328 the baseline simulation at the broadleaved forest site from 2000 to 2024. Groundwater recharge dominates blue
329 water fluxes, while surface runoff is rare and occurs only during extreme summer rainfall events (Figure 4a).
330 Transpiration and canopy evaporation dominate in summer, while soil evaporation peaks in spring. In dry years,
331 recharge declines and dominates the intermonthly variation (Figure 4b), whereas in wet years, it increases
332 following precipitation anomalies (Figure 4c). Despite differences in annual wetness—across both dry and wet
333 years—transpiration remains relatively stable (Figure 4d), indicating resilient vegetation function. This stability
334 likely reflects the mature age of the forest (~60 years), although gradual changes in forest structure over the 20-
335 year period may also play a role. These seasonal patterns offer key insights into water partitioning under broadleaf
336 forest conditions and establish an important baseline for evaluating the impacts of alternative forest management
337 scenarios.



338 **Figure 4.** Mean monthly water balance components for the period 2000–2024, simulated using EcoPlot-iso for a
339 broadleaf forest site in the Demnitzer Millcreek catchment, based on the mean of the best 100 parameter sets (see
340 Section 3.4 for details). (a) Long-term mean monthly water balance. (b) Deviations of dry years (2006, 2018,
341



2022) from the long-term mean. (c) Deviations of wet years (2002, 2007, 2010, 2023) from the long-term mean.
(d) Differences between wet and dry years.

4.3 Impacts of Forest Management on Water Partitioning and Soil Moisture

4.3.1 Water Balance and Partitioning Across Forest Types

Figure 5 compares the mean annual water balance components simulated across broadleaf forest, coniferous forest, and agroforestry types based on the average of the best 100 simulations. LAI was derived from DMC data for each forest type, while the LAI scaling factor and root parameters were kept constant across vegetation types. Results showed that evapotranspiration under coniferous forests accounted for 8% more of annual precipitation than broadleaved forests, and 13% more than in agroforestry systems. This was primarily due to higher transpiration (Tr) and canopy interception evaporation (Ei). In contrast, soil evaporation (Es) and groundwater recharge (Recharge) were lowest in conifers and highest in agroforestry. Agroforestry had 13% more groundwater recharge relative to annual precipitation than conifers, and 4% more than broadleaf forests. Transpiration partitioning across root zones (Tr_Upper, Tr_Lower, Tr_Deep) was similar across all forest types, while surface runoff (Qs) remained minimal and nearly identical. These results reflect the influence of forest structure and canopy cover on ecohydrological partitioning, with coniferous systems favoring atmospheric losses and agroforestry promoting soil evaporation and subsurface recharge. They underscore the trade-offs between evapotranspiration and groundwater recharge across different forest types.

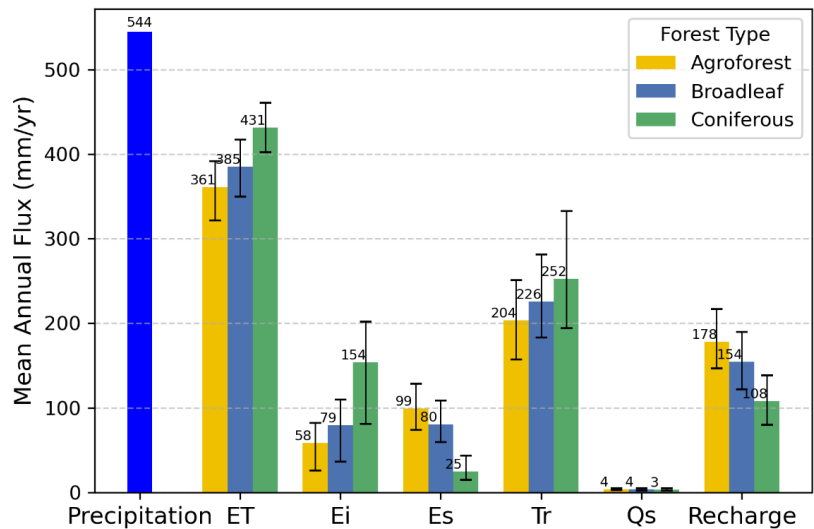
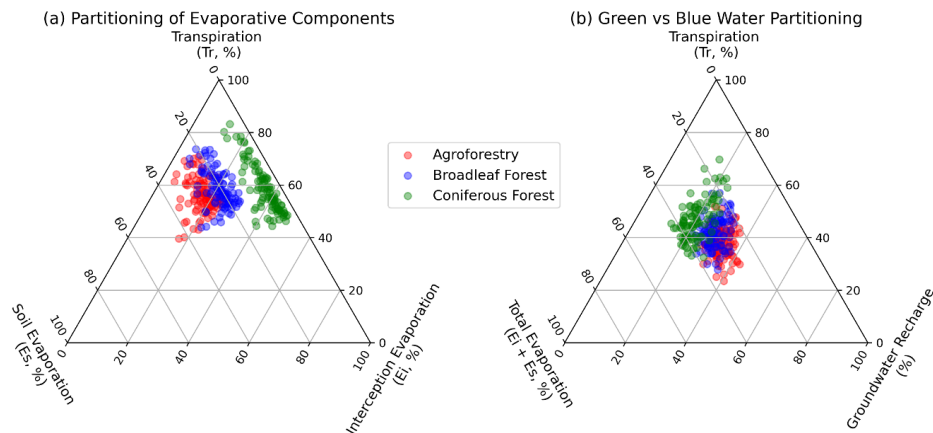


Figure 5. Comparison of mean annual water balance components across different forest types: broadleaf (blue), coniferous (green), and agroforestry (yellow). Bars represent the mean annual flux based on 25-year totals, with error bars indicating the 5th and 95th percentile ranges of the 100 best simulations. All simulations were conducted under baseline conditions with a fixed forest root parameter β of 0 and LAI scaling factor of 1.0.

Figure 6 presents ternary diagrams illustrating the relative partitioning of key water flux components across three forest types under baseline conditions. This shows the predominance in transpiration in all three cases (Fig. 6a). Coniferous forests show a distinct pattern, with the lowest soil evaporation (Es) (Fig. 6a) and groundwater



368 recharge (Fig. 6b) compared to broadleaf and agroforestry systems. In contrast, broadleaf and agroforestry forests
369 display largely overlapping partitioning patterns, except for soil evaporation, which differs notably between the
370 two.



371 **Figure 6.** Water flux partitioning illustrated using ternary plots based on 100 model simulations for three forest
372 types: Agroforestry, Broadleaf Forest, and Coniferous Forest, under baseline conditions (root parameter $\beta = 0$,
373 LAI scaling factor = 1.0). (a) Partitioning of total evapotranspiration into transpiration (Tr), soil evaporation (Es),
374 and interception evaporation (Ei). (b) Partitioning of water fluxes into green water (Tr and $E = Ei + Es$) and blue
375 water (groundwater recharge). Each point represents the normalized annual mean flux from a 25-year simulation.
376 Colored markers denote different forest types.

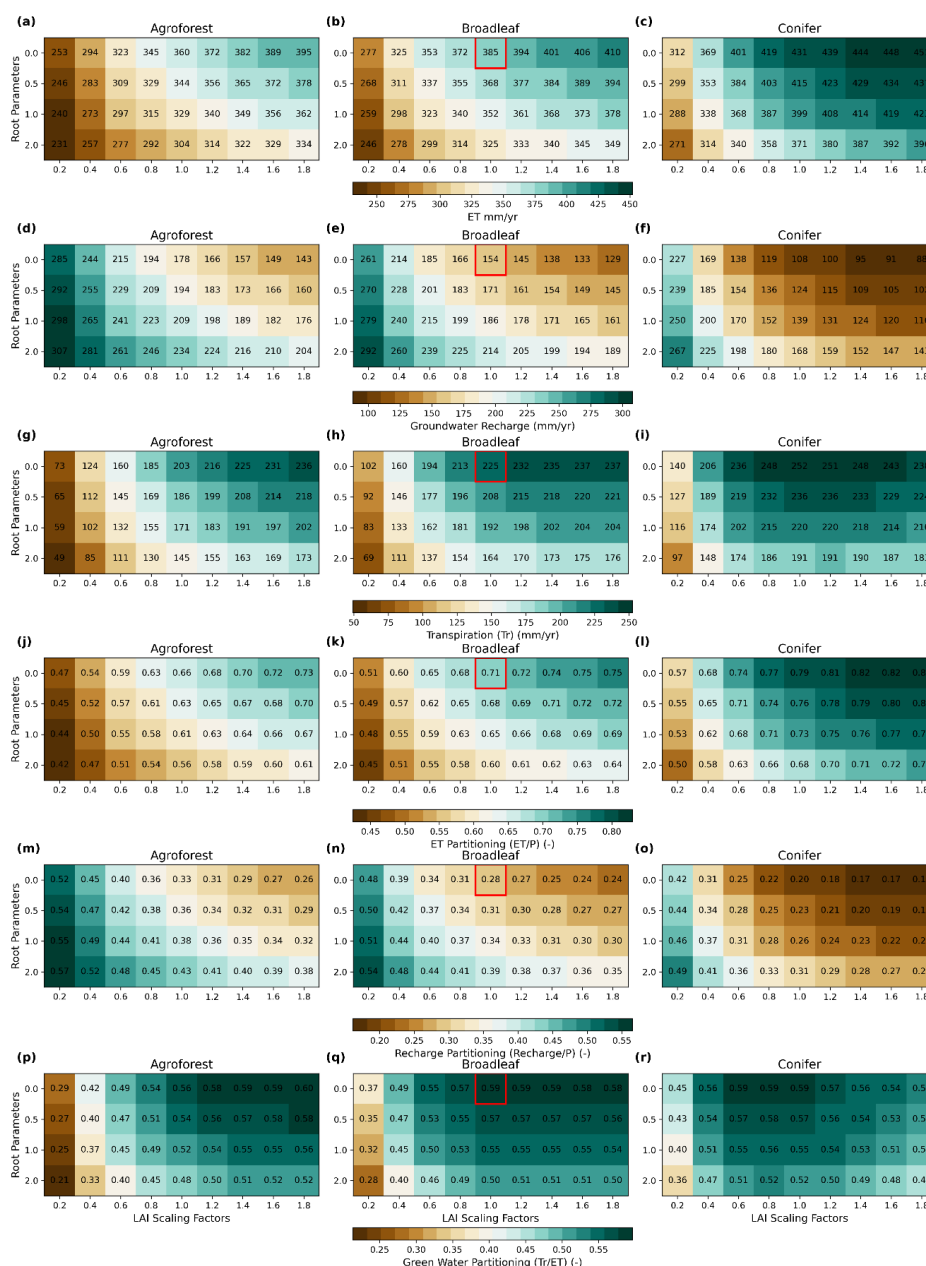
378 4.3.2 Interannual Patterns and Variability of Water Fluxes

379 Figure 7 provides a detailed visualization of the isotope-informed green and blue water partitioning across
380 different forest management scenarios. The heatmaps present the key ecohydrological fluxes, including
381 evapotranspiration (ET) (a–c), groundwater recharge (Recharge) (d–f), transpiration (Tr) (g–i), ET partitioning
382 (ET/P) (j–l), groundwater recharge partitioning (Recharge/P) (m–o) and green water partitioning (Tr/ET) (p–r)
383 for the three forest types: agroforests, broadleaf forests, and coniferous forests. Evapotranspiration (ET) ranges
384 from 231 mm/yr to 453 mm/yr across different scenarios, with ET proportion relative to precipitation varying
385 from 0.42 to 0.83, respectively. In contrast, groundwater recharge ranges from 88 mm/yr to 307 mm/yr.
386 Transpiration (Tr) varies between 49 mm/yr and 238 mm/yr, with the corresponding green water partitioning
387 (Tr/ET) ranging from 0.21 to 0.53. These results underscore the significant influence of vegetation type and
388 structure on ecohydrological fluxes and water partitioning outcomes.

389 Furthermore, annual mean values show that both transpiration and evapotranspiration increase with higher LAI
390 scaling factors, while groundwater recharge decreases (Figure 8). Figures 8a and 8b illustrate the trade-off between
391 increased ET and reduced groundwater recharge under different forest management scenarios. Transpiration and
392 ET rise rapidly at first, then slow down and transpiration even slightly decreases for conifer forests due to soil
393 moisture limitation (Figure 8c). This decline is not observed in broadleaf or agroforestry systems, likely due to
394 their different seasonal LAI patterns. While summer LAI values for broadleaf and coniferous forests may be
395 similar, the consistently high year-round LAI in conifers can exacerbate moisture stress.



396 At higher LAI levels, transpiration decreases slightly while interception and evaporation from the canopy increase
397 (Figure S4). In dense coniferous stands, excessive interception and persistently dry soils limit root water uptake,
398 reducing vegetation function. This highlights a trade-off between transpiration and interception evaporation. The
399 resulting moisture limitation suggests that such high-density forests may not be sustainable under water-limited
400 conditions, as this negative feedback could constrain long-term forest growth and persistence. In addition, forests
401 with shallow-rooted species—such as young trees—tend to transpire less, generate more groundwater recharge,
402 and exhibit lower Tr/ET ratios compared to deep-rooted forests. However, even at constant LAI, transpiration
403 declines with increasing canopy density, suggesting that rooting depth alone cannot compensate for moisture
404 limitations in dense forests.



405

406 **Figure 7.** Green and blue water partitioning across forest types and LAI scaling factors. The heatmaps illustrate
 407 evapotranspiration (ET) (a–c), groundwater recharge (d–f), transpiration (Tr) (g–i), ET partitioning (ET/P) (j–l),
 408 and green water partitioning (Tr/ET) (m–o) for three forest types (Agroforest, Broadleaf, and Conifer). The x-axis
 409 represents scaling factors (forest density), while the y-axis represents root parameters (forest ages). Each heatmap
 410 includes numeric values for clarity, with red-outlined cells indicating the baseline simulations (Broadleaf forest,
 411 scaling factor = 1, root parameter = 0).
 412

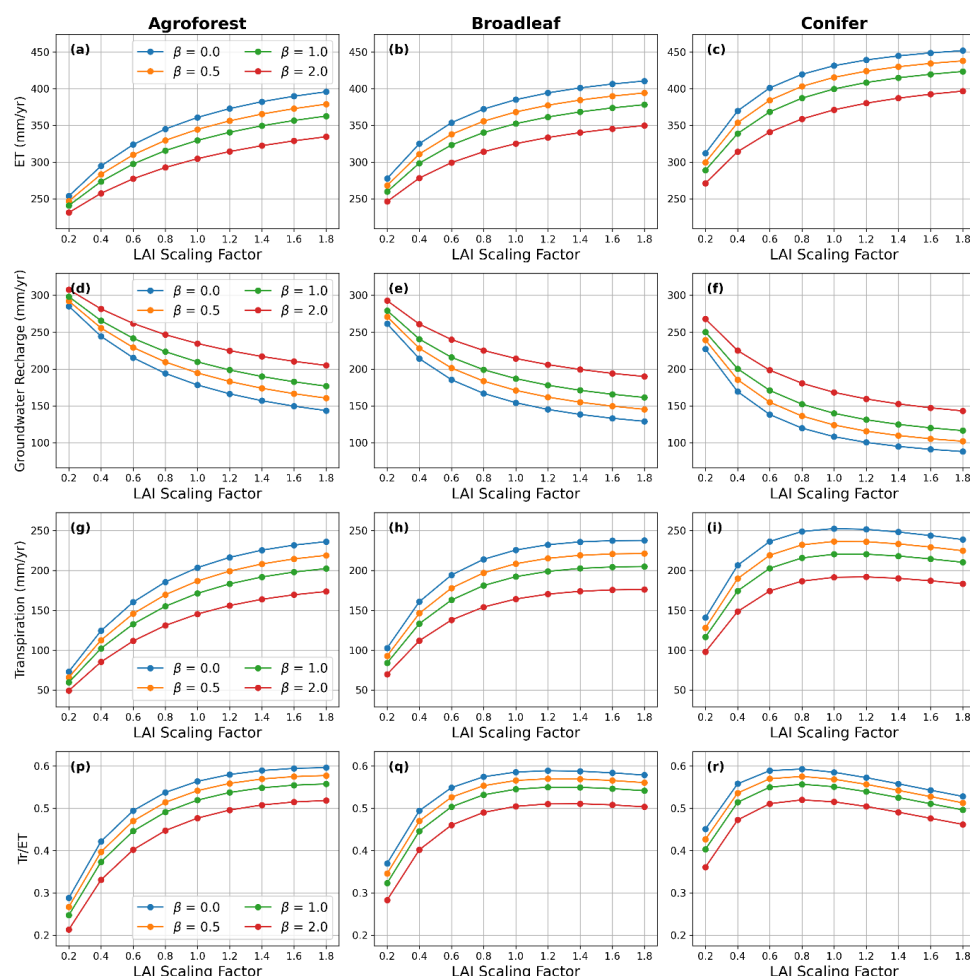


Figure 8. Annual mean ecohydrological fluxes for three forest types (Agroforest, Broadleaf, and Conifer) under varying LAI scaling factors and root depth scenarios. Panels (a)–(c) show evapotranspiration (ET), (d)–(f) show groundwater recharge, (g)–(i) show transpiration, and (p)–(r) show the ratio of transpiration to total evapotranspiration (Tr/ET). Each line represents a different forest age class (i.e., root depth) denoted by β values.

4.3.3 Seasonal and Monthly Dynamics of Water Fluxes

Figure 9 shows monthly deviations in water balance components under different forest management scenarios, relative to a baseline broadleaf forest. Agroforestry scenarios tend to have lower transpiration and canopy evaporation, but higher soil evaporation during summer (Fig. 9a). They are also associated with greater groundwater recharge from summer through the following winter. A shift from broadleaf to conifer forests is expected to have a greater impact on the water balance than the shift from agroforest to broadleaf (Fig. 9a and 9b). Compared to broadleaf forests, conifer forests exhibit higher simulated transpiration in March (Fig. 9b), driven by increased potential evapotranspiration and a relatively higher leaf area index (LAI) under wet soil conditions. This difference diminishes as the LAI of broadleaf forests increases in spring.



429 Changes in the LAI scaling factor influence water balance components in summer, increasing transpiration and
430 canopy evaporation while reducing recharge and soil evaporation (Fig. 9c and 9d). Increasing the LAI scaling
431 factor from 0.4 to 1.0 has a greater impact than reducing it from 1.6 to 1.0, as vegetation water use responds more
432 sensitively at low LAI values but plateaus at higher values due to energy or soil moisture limitations. Altering the
433 forest root parameter (β), while using the same LAI time series, primarily affects deep-layer transpiration,
434 reducing total transpiration and increasing recharge. Other water balance components remain unchanged because
435 the LAI time series is held constant.

436 Figure 10 illustrates the relative monthly deviations in evapotranspiration (ET) and groundwater recharge under
437 varying forest types, LAI scaling factors, and root distributions, relative to a baseline broadleaf forest.
438 Agroforestry increases recharge during the low-flow season (June–December) (Fig. 10a), while conifer forests
439 consistently reduce recharge and exhibit substantially higher ET in winter (Fig. 10b). The effects of LAI scaling
440 are most pronounced during the low-flow season. A higher LAI (scaling factor = 1.6) increases ET and reduces
441 recharge, whereas a lower LAI (scaling factor = 0.4) has the opposite effect. However, at higher LAI values, the
442 magnitude of relative deviation diminishes, suggesting a saturation effect. Root distribution also affects seasonal
443 water balance. Scenarios with deeper roots tend to reduce recharge, while shallow root systems enhance recharge
444 during dry months across all forest types. Overall, these results highlight the sensitivity of summer water balance
445 to vegetation structure. Agroforestry consistently exhibits more ecohydrologically resilient responses than conifer
446 forests, particularly under drought-sensitive conditions.

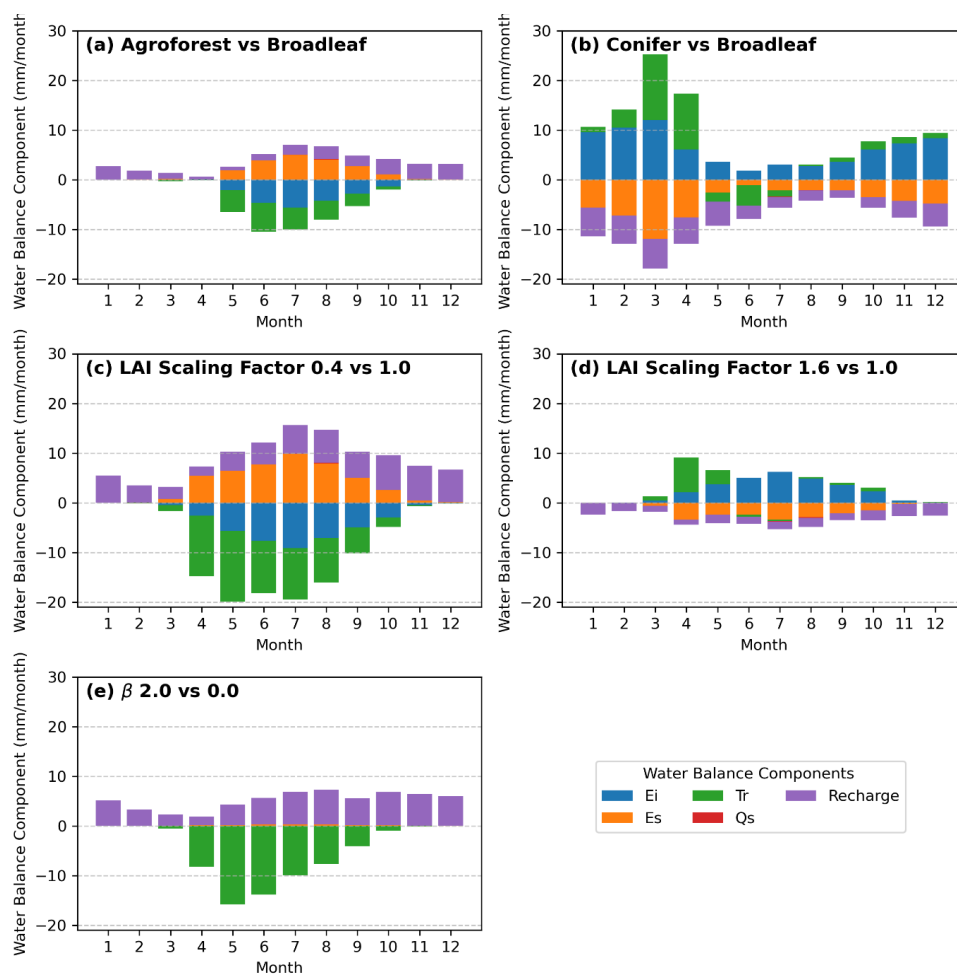


Figure 9. Monthly deviations of water balance components relative to the baseline broadleaf forest scenario. Each panel illustrates the deviation of monthly water balance components from the baseline simulation, with only one parameter modified in each scenario: (a) Agroforest, (b) Conifer forest, (c) LAI scaling factor = 0.4, (d) LAI scaling factor = 1.6, and (e) Root parameter β = 2.0. Tr: transpiration, Ei: canopy evaporation, Es: soil evaporation, Qs: surface runoff, Recharge: groundwater recharge.

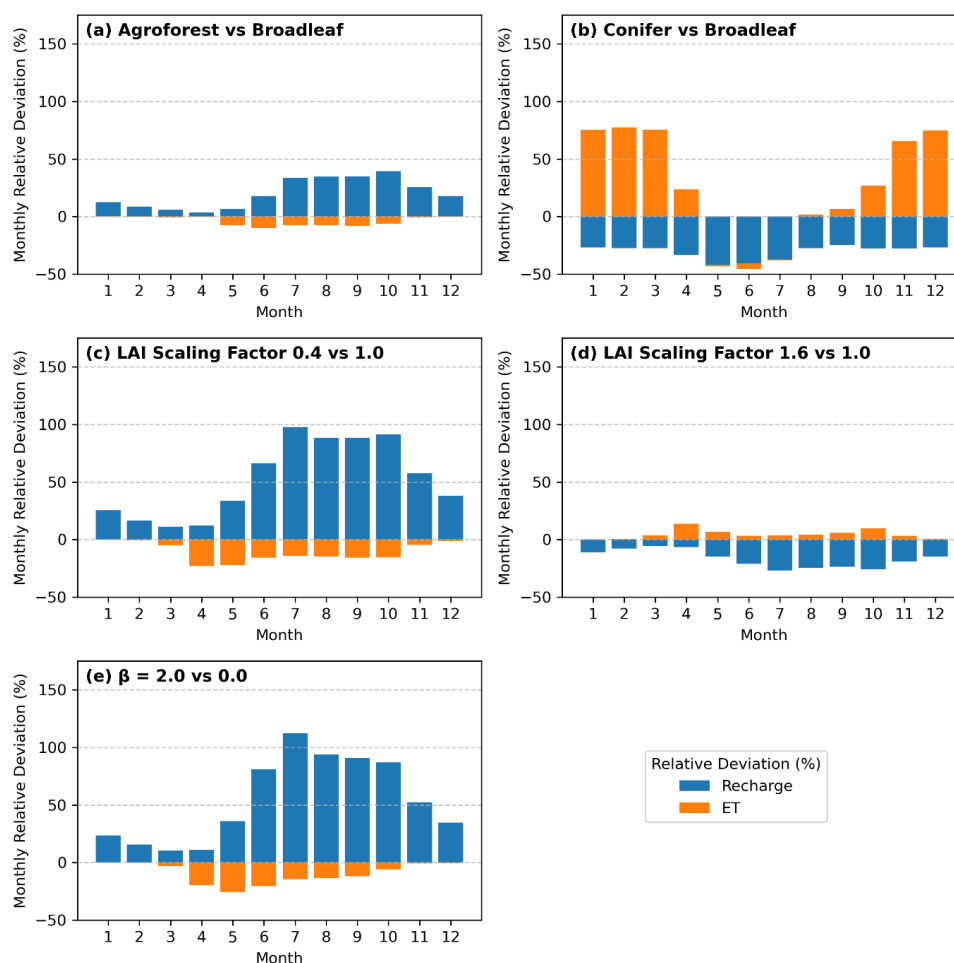


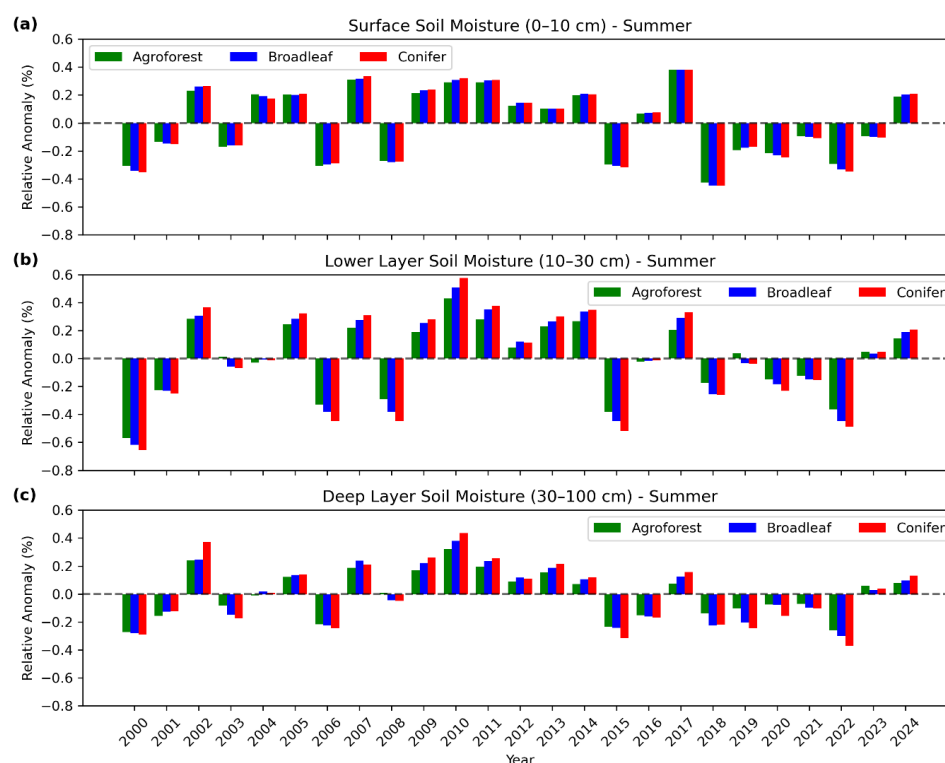
Figure 10. Monthly relative deviations in evapotranspiration (ET) and groundwater recharge, calculated as (scenario - baseline)/baseline $\times 100\%$, relative to the baseline broadleaf forest simulation. Each panel represents a different scenario in which one variable is modified while others are held constant: (a) Agroforest vs Broadleaf, (b) Conifer vs Broadleaf, (c) LAI scaling 0.4 vs 1.0, (d) LAI scaling 1.6 vs 1.0, and (e) Root parameter $\beta = 2.0$ vs 0.0.

4.3.4 Soil Moisture Anomalies

Figure 11 shows the relative summer soil moisture anomalies across three forest types and three soil layers. Anomalies are calculated as the percentage deviation from the long-term seasonal mean, enabling normalized comparison across forest types and soil layers. Conifer forests exhibit the strongest soil moisture anomalies, followed by broadleaf forests, while agroforests exhibit the least variability, indicating greater stability in soil moisture. Furthermore, among the three soil layers, the intermediate layer (10–30 cm) consistently shows stronger anomalies across all forest types, with magnitudes nearly double those of the other layers, highlighting its vulnerability during summer drought. In contrast, the surface layer (0–10 cm) and deep layer (30–100 cm) exhibit weaker anomalies, likely due to frequent soil moisture replenishment by summer rainfall in the surface layer and either more stable moisture retention or greater water storage capacity at depth that compensates for drought.



470 impacts. Negative soil moisture anomalies are more pronounced in summer than in spring, reflecting the stronger
471 seasonal drought effects and fluctuations in soil moisture (see Figure S5 in the Supplementary Material). During
472 spring, broadleaf forests and agroforests display similar negative soil moisture anomalies, suggesting comparable
473 seasonal soil moisture dynamics between these forest types (Figure S5).



474 **Figure 11.** Relative soil moisture anomalies for summer (June–August) across three soil layers: (a) surface (0–10
475 cm), (b) lower layer (10–30 cm), and (c) deep layer (30–100 cm) for three forest types (Agroforest, Broadleaf,
476 Conifer). Bars represent deviations from the long-term mean, with positive values indicating wetter conditions
477 and negative values indicating drier conditions.
478

479 5 Discussion

480 5.1 Implications of Forest Management Scenarios for Water Availability and Water Resource Management

481 Assessing the influence of different land use types on water availability is inherently challenging due to the
482 complex interactions among vegetation, climate, and soil properties (te Wierik et al., 2021; Zhang et al., 2001).
483 Different vegetation types have distinct water demands, and their contrasting canopy structures affect how
484 precipitation is intercepted, and partitioned into infiltration, runoff, groundwater recharge, and evapotranspiration
485 (Brauman et al., 2010). Vegetation management practices can significantly alter these processes. Moreover, the
486 effects of vegetation and canopy structure may vary depending on underlying soil characteristic (Geris et al.,
487 2015). This complexity poses a significant challenge for land managers and policymakers, especially in drought-
488 sensitive regions facing increasing aridity due to climate change (Orth & Destouni, 2018). In such contexts,



489 providing informed guidance on sustainable land cover choices is increasingly important to maintain long-term
490 water availability (Estrela & Vargas, 2012). In regions where forestry has traditionally been an important land use,
491 shifting hydroclimatic conditions underscore the need to assess the resilience of different forest types and
492 management practices (Quandt et al., 2023). This requires evaluating water yield across multiple temporal scales,
493 including how forest management affects annual and seasonal water partitioning, and its implications for residual
494 water availability—specifically streamflow generation and groundwater recharge during low-flow periods
495 (Brown et al., 2005; Neill et al., 2021).

496 Although complex, process-based ecohydrological models such as RHESSys and EcH₂O can capture detailed
497 interactions among hydrological processes and water fluxes in data-rich research settings, their broader application
498 in forest and land management is often limited by the high data requirements for model forcing and calibration
499 (Fatichi et al., 2012; Kuppel et al., 2018; Tague & Band, 2004). In this study, we sought to apply a parsimonious
500 tracer-aided modelling approach to provide insights into the effects of different forest management scenarios on
501 water partitioning and land use resilience in Brandenburg, northeastern Germany, where recent droughts have
502 shown that traditional forest management practices focused on coniferous plantations of Scots pine may not be
503 sustainable (Luo et al., 2024). By employing the tracer-aided ecohydrological model EcoPlot-iso, we used a
504 generic approach to help quantify the long-term impacts of variations in forest type, stand density and root depth
505 distribution on both blue and green water fluxes.

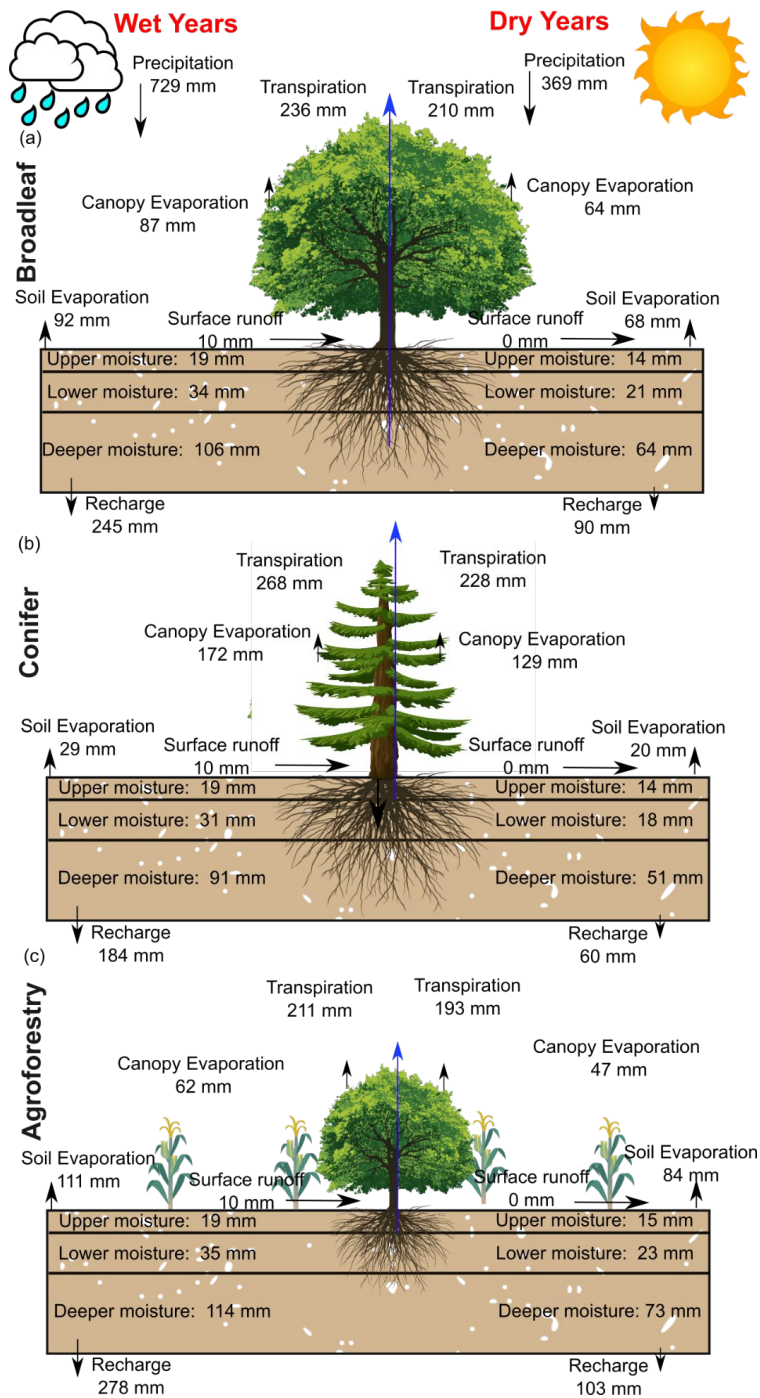
506 In the baseline simulation for mature broadleaved forest, the estimated mean annual evapotranspiration (ET) for
507 or 2000–2024 was 390 mm/year, accounting for 72% of annual precipitation. This value is consistent with ET
508 estimates reported in previous modelling at DMC in 2021, ranging from 68% to over 80% of annual precipitation
509 (Landgraf et al., 2023), 2018–2020 (Smith et al., 2021). The discrepancy may reflect interannual climate
510 variability and the influence of particularly dry or wet years that cannot be captured by short-term assessments.
511 Differences in model structure, parameterization, and input data may also contribute to the spread in ET values.
512 Nonetheless, this comparison underscores the importance of long-term simulations for capturing representative
513 hydrological behavior and evaluating the impacts of forest management strategies under variable climatic
514 conditions.

515 In catchments like DMC, where evapotranspiration (ET) is high, atmospheric demand is the primary driver of root
516 water uptake, though vegetation plays a key role in regulating its impact on water availability. In Brandenburg,
517 coniferous forests have traditionally been favored on sandy soils, but modelling indicates high water use due to
518 interception losses and year-round transpiration potential (Fig. 9). Consequently, the implications for both reduced
519 groundwater recharge and reduced forest productivity has encouraged landowners to explore alternative land use,
520 such as broadleaves forests and agroforestry. These options have the potential for optimizing biomass productivity
521 and land use resilience with increased landscape water retention and increased groundwater recharge.

522 These results (e.g., Figs. 7 and 8) have practical applications, such as estimating the direction and magnitude of
523 the changes in evapotranspiration and water yield as a function of forest management practices, driven by
524 alterations in canopy structure and rooting depth. The modelling approach thus provides useful insights into the
525 hydrological implications of alternative canopy structures and rooting patterns for water use. Figure 12 compares
526 the mean annual partitioning of water fluxes and soil moisture across broadleaf, coniferous, and agroforest types
527 under dry and wet year conditions. It highlights how different vegetation strategies influence hydrological



528 resilience, with substantial differences in water partitioning observed between dry and wet years across contrasting
529 forest management scenarios. By simulating long-term water availability across periods of alternating wet and dry
530 conditions, EcoPlot-iso simulations suggest that mixed forests and agroforestry can enhance water supply
531 resilience in drought-sensitive catchments by sustaining both water yield and groundwater recharge.
532



533
534 **Figure 12.** Comparison of mean annual water fluxes and soil moisture in the upper, lower, and deeper layers for
535 Broadleaf (a), Coniferous (b), and Agroforest (c) forests under dry (2006, 2018, 2022) and wet (2002, 2007,
536 2010, 2023) year conditions.



5.2 Soil Moisture Anomalies and Their Implications for Resilience

At most of the monitoring plots in the DMC, groundwater is typically more than 3 meters below the ground surface (Ying et al., 2025). Therefore, except in older forest plots with deeply rooting trees, vegetation relies on soil moisture for root water uptake. Even for mature trees, there is evidence that most root water uptake occurs in the near-surface soil horizons, as demonstrated by (Birkel et al., 2025), 20 km from the DMC. A global synthesis by Evaristo & McDonnell (2017) further supports this, indicating that ~77% of plant water uptake comes from shallow sources, with deeper groundwater use primarily in more arid regions. While hydraulic redistribution may provide deeper access for some species (Emerman & Dawson, 1996), rooting strategies are complex and highly species-specific (Demir et al., 2024). In this context, our results highlight the intermediate soil layer (10–30 cm) as the most reactive and significant for sustaining transpiration, with anomaly magnitudes nearly twice those of both the shallow (0–10 cm) and deeper (30–60 cm) layers across all forest types.

In addition, seasonal comparisons revealed that summer soil moisture anomalies were more negative than those in spring for all forest types (Figure S5). This is likely linked to higher temperatures and evapotranspiration during summer, which intensify water stress and drive seasonal variation in soil moisture availability. Forest density and rooting characteristics substantially influenced the relative magnitude of soil moisture anomalies (Figure S6 and S7, respectively). Denser forests exhibited stronger negative anomalies during dry periods and enhanced positive anomalies in wet periods, amplifying seasonal fluctuations. For example, high-density (LAI scaling factor 1.6) conifer stands showed relative anomalies up to 25% greater than their low-density counterparts (Figure S7). In contrast, shallow-rooted systems moderated this response, leading to more stable soil moisture dynamics. Among the management scenarios, agroforestry consistently exhibited the smallest anomalies, reflecting greater buffering capacity and higher ecohydrological resilience.

The improved rooting scheme in EcoPlot-iso represents depth-dependent transpiration by dynamically linking root water uptake efficiency to soil moisture availability across three soil compartments (see Section 3.2). Unlike models such as RHESSys and ECH2O, which partition a prescribed total transpiration—typically derived from the energy balance—across layers based on static root distributions, our approach allows transpiration to emerge from potential evapotranspiration, root-zone constraints, and soil moisture availability. The aim was not to optimize species-specific root dynamics, but to represent the relative influence of rooting depth on water uptake and partitioning, particularly in shallow-rooted or structurally diverse systems such as young forests. While the new implementation improves the process representation of root–soil interactions, it did not result in a substantial improvement in simulated soil moisture. For shallow vegetation types such as grasslands and croplands, model performance—measured using the mKGE was similar with and without the new transpiration function (results not shown). Moreover, direct validation of the root uptake scheme remains challenging due to the lack of supporting observations, such as root distribution data, xylem water isotopes, or sap flux measurements. Addressing this issue is a clear priority for future research.

These findings highlight how structurally diverse systems, such as agroforests, enhance the buffering capacity of ecosystems by improving groundwater recharge and reducing the amplitude of soil moisture fluctuations, thereby supporting greater resilience during dry periods (Tetzlaff et al., 2024). Together, these insights underscore the importance of rooting depth, forest structure, and seasonal climate variability in shaping soil moisture patterns



575 and regulating vegetation resilience. Accounting for these factors is essential for informing adaptive forest
576 management in drought-prone catchments like the DMC.

577 **5.3 Advancing Tracer-Aided Ecohydrological Modeling: Challenges and Future Outlook**

578 This study demonstrates that tracer-aided ecohydrological models, such as the isotope-aided EcoPlot-iso, can
579 effectively quantify the impact of forest management scenarios on water partitioning and ecohydrological
580 resilience. By distinguishing between evaporation, transpiration, and subsurface water movements using stable
581 isotopes (Tetzlaff & Soulsby, 2008), the model captures key hydrological responses—including
582 evapotranspiration (ET), groundwater recharge, and soil moisture dynamics—under varying management
583 strategies. These insights support evidence-based decision-making in drought-sensitive landscapes.

584 Despite these advances, several challenges remain. Conducted in a 66 km² mid-sized basin, this study did not
585 include land use change induced atmospheric feedbacks—such as changes in albedo, radiative balance, or rainfall
586 patterns—which are less critical at this scale but become important in larger-scale modeling (Ellison et al., 2012;
587 Filoso et al., 2017). Moreover, this study applied a multi-objective calibration approach, combined with Monte
588 Carlo sampling, that equally weighted isotopic and soil moisture data. However, further investigation is needed
589 in how these observational constraints are balanced and interpreted. Recent advances—such as the
590 DREAM(LoAX) framework (Wu et al., 2025)—demonstrate how simultaneous calibration and diagnostic
591 analysis under the equifinality thesis can improve parameter identifiability, model robustness, and process
592 understanding in tracer-aided ecohydrological models.

593 Many recent studies have used isotopic data to investigate root water uptake patterns, revealing how tree species,
594 soil properties, and spatial water availability shape plant water use strategies (Demir et al., 2024; Rothfuss &
595 Javaux, 2017). Integrating tracer-aided models with soil and xylem water isotope data offers a promising path to
596 improving the representation of root water uptake, which is often simplified in current modelling approaches
597 (Birkel et al., 2025). Improving root uptake representation requires consideration of species-specific traits and
598 local soil-water conditions. However, the practical application of such improvements is limited by the scarcity of
599 soil and xylem water isotope data, which are essential for constraining root water uptake dynamics but remain
600 rare due to the labor-intensive and technically demanding nature of field sampling and laboratory analysis
601 (Landgraf et al., 2022; Sprenger et al., 2017). This scarcity hinders the spatial and temporal resolution of
602 observational data, limiting our ability to refine root water uptake processes in tracer-aided models.

603 Upscaling from plot to landscape level remains complex due to spatial heterogeneity in vegetation, soils, and
604 topography. Addressing this requires spatially distributed modeling frameworks that can explicitly capture
605 heterogeneity in ecohydrological processes across different landscape units (Kuppel et al., 2018; van Huijgevoort
606 et al., 2016). Enhanced integration with remote sensing techniques can also help address these scaling limitations
607 by providing spatially continuous data on vegetation dynamics, soil moisture, and ET (Yang et al., 2023).
608 Incorporating ET observations, for instance, could strengthen model interpretation of flux dynamics. Currently,
609 key processes such as lateral subsurface flows and upward capillary fluxes are not explicitly represented in the
610 EcoPlot-iso model. Including these components, along with improved representation of groundwater-surface
611 water interactions, could improve simulations of water connectivity and storage resilience.



612 Future development should emphasize the coupling of tracer-based approaches with high-resolution hydrological
613 modeling, remote sensing data, isotope data, and empirical field studies. Such interdisciplinary integration is
614 essential for improving the scalability and applicability of tracer-aided ecohydrological models, especially for
615 informing sustainable forest and water management under uncertain hydroclimatic futures.

616 **6 Conclusion and Outlook**

617 The isotope-aided EcoPlot-iso modelling framework was applied to quantify the impacts of different forest
618 management strategies on water partitioning and ecohydrological resilience in the drought-sensitive Demnitzer
619 Millcreek catchment in northeastern Germany. The model was first set up and evaluated under a baseline
620 simulation for the period 2000–2024 at a broadleaf reference site, successfully reproducing observed soil moisture
621 and soil water isotope dynamics using a multi-objective calibration approach. A novel depth-dependent root water
622 uptake function was integrated, and a suite of scenario simulations—varying in forest type, canopy density, and
623 rooting depth—was conducted to assess changes in evapotranspiration, groundwater recharge, and soil moisture
624 anomalies under both dry and wet climatic conditions.

625 The results revealed clear trade-offs between evapotranspiration (ET) and groundwater recharge, depending on
626 forest management strategies. Coniferous forests intensified drought impacts, with approximately 8–13% higher
627 ET compared to broadleaf and agroforestry systems, and significantly reduced groundwater recharge, particularly
628 during low-flow dry periods. In contrast, agroforestry systems effectively buffered drought stress and maintaining
629 lower soil moisture variability, which simultaneously lowering ET and enhancing groundwater recharge by about
630 13%. Further analysis highlighted contrasting ecosystem responses: conifers showed the strongest soil moisture
631 anomalies, indicating greater drought sensitivity, while agroforests exhibited the most stable soil water storage.
632 The intermediate soil layer (10–30 cm) was identified as the most responsive zone, consistently exhibiting the
633 largest anomalies due to its role as the dominant root water uptake region supporting transpiration.

634 Beyond advancing process understanding, this study provided practical tools for land management. By
635 incorporating key controls such as canopy properties and root distribution, EcoPlot-iso facilitates an accessible
636 means of assessing long-term land management impacts on landscape ecohydrology. The visualization and
637 decision-support framework developed here offers a transparent, scenario-based platform for evaluating forest
638 management strategies in climate-sensitive regions. These tools are well-suited for informing resilient land use
639 planning under increasing climate variability.

640 Looking ahead, future research could usefully aim to incorporate additional isotopic tracers—such as deeper soil
641 water (> 1 m), groundwater, and xylem water isotopes—to further constrain root water uptake functions and
642 capture their variability across species and hydroclimatic conditions. The integration of high-resolution remote
643 sensing data—particularly LiDAR for detailed characterization of forest structure—will enhance model
644 parameterization and improve the spatial representation of heterogeneity in canopy height, leaf area distribution,
645 and forest density. Advancing the EcoPlot-iso framework to incorporate lateral subsurface flows, groundwater
646 dynamics, and coupled land–atmosphere feedbacks will support broader applications, including the assessment of
647 large-scale land use change. Collectively, these developments will enhance model robustness and enable more
648 informed, resilient land and water management strategies under a warming climate.



649 **Code and data availability**

650 The data and code that support the findings of this study are available from the corresponding author upon
651 reasonable request.

652 **Author contribution**

653 CJ contributed to the methodology, software development, formal analysis, investigation, visualization, and
654 writing of the original draft. DT contributed to conceptualization, investigation, data curation, validation,
655 resources, project administration, and funding acquisition. SW contributed to methodology, investigation and data
656 curation. CB contributed to software, methodology, and resources. HL contributed to investigation, visualization
657 and validation. CS contributed to conceptualization, methodology, validation, investigation. All authors
658 contributed to writing – review and editing.

659 **Competing interests**

660 The authors declare that they have no conflict of interest.

661 **Acknowledgements**

662 Tetzlaff's contributions were partly funded through the WETSCAPES2.0 project (DFG TRR410/1 2025). Tetzlaff
663 also received funding from the "Wasserressourcenpreis 2024" awarded by the Rüdiger Kurt Bode-Foundation.
664 Contributions from Soulsby were supported by Leibnitz Association Germany in the project Wetland Restoration
665 in Peatlands. Laudon was funded by KAW 2018.0259 and 2023.0245, and Soulsby was also funded as an
666 International KSLA Guest Professor at SLU by the Wallenberg Foundation (WP2023-0001). Birkel would like to
667 thank the IGB for generously supporting him with a senior fellowship and the UCR for a sabbatical license. We
668 extend our appreciation to Benedikt Boesel and the team from the Finck Foundation (www.finck-stiftung.org) for
669 their collaborative support and for granting access to study sites.

670 **Reference**

- 671 Ault, T. R. (2020). On the essentials of drought in a changing climate. In *Science* (Vol. 368, Issue 6488).
672 <https://doi.org/10.1126/science.aaz5492>
- 673 Birkel, C., Arciniega-Esparza, S., Maneta, M. P., Boll, J., Stevenson, J. L., Benegas-Negri, L., Tetzlaff, D., &
674 Soulsby, C. (2024). Importance of measured transpiration fluxes for modelled ecohydrological partitioning
675 in a tropical agroforestry system. *Agricultural and Forest Meteorology*, 346.
676 <https://doi.org/10.1016/j.agrformet.2023.109870>
- 677 Birkel, C., Tetzlaff, D., Ring, A. M., & Soulsby, C. (2025). Does high resolution in situ xylem and atmospheric
678 vapor isotope data help improve modeled estimates of ecohydrological partitioning? *Agricultural and*
679 *Forest Meteorology*, 365. <https://doi.org/10.1016/j.agrformet.2025.110467>



- 680 Bonan, G. B. (2008). Forests and climate change: Forcings, feedbacks, and the climate benefits of forests. In
681 *Science* (Vol. 320, Issue 5882). <https://doi.org/10.1126/science.1155121>
- 682 Bosch, J. M., & Hewlett, J. D. (1982). A REVIEW OF CATCHMENT EXPERIMENTS TO DETERMINE THE
683 EFFECT OF VEGETATION CHANGES ON WATER YIELD AND EVAPOTRANSPIRATION. In
684 *Journal of Hydrology* (Vol. 55).
- 685 Brauman, K. A., Freyberg, D. L., & Daily, G. C. (2010). Forest structure influences on rainfall partitioning and
686 cloud interception: A comparison of native forest sites in Kona, Hawai'i. *Agricultural and Forest*
687 *Meteorology*, 150(2). <https://doi.org/10.1016/j.agrformet.2009.11.011>
- 688 Brown, A. E., Western, A. W., McMahon, T. A., & Zhang, L. (2013). Impact of forest cover changes on annual
689 streamflow and flow duration curves. *Journal of Hydrology*, 483.
690 <https://doi.org/10.1016/j.jhydrol.2012.12.031>
- 691 Brown, A. E., Zhang, L., McMahon, T. A., Western, A. W., & Vertessy, R. A. (2005). A review of paired
692 catchment studies for determining changes in water yield resulting from alterations in vegetation. *Journal*
693 *of Hydrology*, 310(1–4), 28–61. <https://doi.org/10.1016/j.jhydrol.2004.12.010>
- 694 Calder, I. R. (1998). Water use by forests, limits and controls. *Tree Physiology*, 18(8–9).
695 <https://doi.org/10.1093/treephys/18.8-9.625>
- 696 Demir, G., Guswa, A. J., Filipzik, J., Metzger, J. C., Römermann, C., & Hildebrandt, A. (2024). Root water uptake
697 patterns are controlled by tree species interactions and soil water variability. *Hydrology and Earth System*
698 *Sciences*, 28(6), 1441–1461. <https://doi.org/10.5194/hess-28-1441-2024>
- 699 Douinot, A., Tetzlaff, D., Maneta, M., Kuppel, S., Schulte-Bisping, H., & Soulsby, C. (2019). Ecohydrological
700 modelling with ECH2O-iso to quantify forest and grassland effects on water partitioning and flux ages.
701 *Hydrological Processes*, 33(16), 2174–2191. <https://doi.org/10.1002/hyp.13480>
- 702 Dubbert, M., Couvreur, V., Kübert, A., & Werner, C. (2023). Plant water uptake modelling: added value of cross-
703 disciplinary approaches. In *Plant Biology* (Vol. 25, Issue 1). <https://doi.org/10.1111/plb.13478>
- 704 Ellison, D., Futter, M. N., & Bishop, K. (2012). On the forest cover-water yield debate: From demand- to supply-
705 side thinking. In *Global Change Biology* (Vol. 18, Issue 3). <https://doi.org/10.1111/j.1365-2486.2011.02589.x>
- 707 Emerman, S. H., & Dawson, T. E. (1996). Hydraulic lift and its influence on the water content of the rhizosphere:
708 An example from sugar maple, *Acer saccharum*. *Oecologia*, 108(2). <https://doi.org/10.1007/BF00334651>
- 709 Estrela, T., & Vargas, E. (2012). Drought Management Plans in the European Union. The Case of Spain. In *Water*
710 *Resources Management* (Vol. 26, Issue 6). <https://doi.org/10.1007/s11269-011-9971-2>
- 711 Evaristo, J., & McDonnell, J. J. (2017). Prevalence and magnitude of groundwater use by vegetation: A global
712 stable isotope meta-analysis. *Scientific Reports*, 7. <https://doi.org/10.1038/srep44110>
- 713 Falkenmark, M., & Rockström, J. (2006). The New Blue and Green Water Paradigm: Breaking New Ground for
714 Water Resources Planning and Management. *Journal of Water Resources Planning and Management*,
715 132(3). [https://doi.org/10.1061/\(asce\)0733-9496\(2006\)132:3\(129\)](https://doi.org/10.1061/(asce)0733-9496(2006)132:3(129))



- 716 Fatichi, S., Ivanov, V. Y., & Caporali, E. (2012). A mechanistic ecohydrological model to investigate complex
717 interactions in cold and warm water-controlled environments: 1. Theoretical framework and plot-scale
718 analysis. *Journal of Advances in Modeling Earth Systems*, 4(5). <https://doi.org/10.1029/2011MS000086>
- 719 Filoso, S., Bezerra, M. O., Weiss, K. C. B., & Palmer, M. A. (2017). Impacts of forest restoration on water yield:
720 A systematic review. In *PLoS ONE* (Vol. 12, Issue 8). <https://doi.org/10.1371/journal.pone.0183210>
- 721 Gelbrecht, J., Driescher, E., Lademann, H., Schönfelder, J., & Exner, H.-J. (1996). Diffuse nutrient impact on
722 surface water bodies and its abatement by restoration measures in a small catchment area in North-East
723 Germany. *Water Science and Technology*, 33(4–5). <https://doi.org/10.2166/wst.1996.0501>
- 724 Gelbrecht, J., Lengsfeld, H., Pöthig, R., & Opitz, D. (2005). Temporal and spatial variation of phosphorus input,
725 retention and loss in a small catchment of NE Germany. *Journal of Hydrology*, 304(1–4), 151–165.
726 <https://doi.org/10.1016/j.jhydrol.2004.07.028>
- 727 Geris, J., Tetzlaff, D., McDonnell, J., & Soulsby, C. (2015). The relative role of soil type and tree cover on water
728 storage and transmission in northern headwater catchments. *Hydrological Processes*, 29(7).
729 <https://doi.org/10.1002/hyp.10289>
- 730 Guswa, A. J., Tetzlaff, D., Selker, J. S., Carlyle-Moses, D. E., Boyer, E. W., Bruen, M., Cayuela, C., Creed, I. F.,
731 van de Giesen, N., Grasso, D., Hannah, D. M., Hudson, J. E., Hudson, S. A., Iida, S., Jackson, R. B., Katul,
732 G. G., Kumagai, T., Llorens, P., Lopes Ribeiro, F., ... Levia, D. F. (2020). Advancing ecohydrology in the
733 21st century: A convergence of opportunities. In *Ecohydrology* (Vol. 13, Issue 4). John Wiley and Sons Ltd.
734 <https://doi.org/10.1002/eco.2208>
- 735 Hersbach, H., Bell, B., Berrisford, P., Hirahara, S., Horányi, A., Muñoz-Sabater, J., Nicolas, J., Peubey, C., Radu,
736 R., Schepers, D., Simmons, A., Soci, C., Abdalla, S., Abellan, X., Balsamo, G., Bechtold, P., Biavati, G.,
737 Bidlot, J., Bonavita, M., ... Thépaut, J.-N. (2020). The ERA5 global reanalysis. *Quarterly Journal of the*
738 *Royal Meteorological Society*, 146(730), 1999–2049. <https://doi.org/10.1002/qj.3803>
- 739 Hibbert, A. R. (1967). Forest Treatment Effects on Water Yield. *International Symposium For Hydrology*.
- 740 Huntington, T. G. (2006). Evidence for intensification of the global water cycle: Review and synthesis. *Journal*
741 *of Hydrology*, 319(1–4), 83–95. <https://doi.org/10.1016/j.jhydrol.2005.07.003>
- 742 Kleine, L., Tetzlaff, D., Smith, A., Dubbert, M., & Soulsby, C. (2021). Modelling ecohydrological feedbacks in
743 forest and grassland plots under a prolonged drought anomaly in Central Europe 2018–2020. *Hydrological*
744 *Processes*, 35(8). <https://doi.org/10.1002/hyp.14325>
- 745 Kling, H., Fuchs, M., & Paulin, M. (2012). Runoff conditions in the upper Danube basin under an ensemble of
746 climate change scenarios. *Journal of Hydrology*, 424–425. <https://doi.org/10.1016/j.jhydrol.2012.01.011>
- 747 Knighton, J., Kuppel, S., Smith, A., Soulsby, C., Sprenger, M., & Tetzlaff, D. (2020). Using isotopes to
748 incorporate tree water storage and mixing dynamics into a distributed ecohydrologic modelling framework.
749 *Ecohydrology*, 13(3). <https://doi.org/10.1002/eco.2201>



- 750 Knighton, J., Sanchez-Martinez, P., & Anderegg, L. (2024). A global dataset of tree hydraulic and structural traits
751 imputed from phylogenetic relationships. *Scientific Data*, 11(1). [https://doi.org/10.1038/s41597-024-](https://doi.org/10.1038/s41597-024-04254-4)
752 04254-4
- 753 Kool, D., Agam, N., Lazarovitch, N., Heitman, J. L., Sauer, T. J., & Ben-Gal, A. (2014). A review of approaches
754 for evapotranspiration partitioning. In *Agricultural and Forest Meteorology* (Vol. 184).
755 <https://doi.org/10.1016/j.agrformet.2013.09.003>
- 756 Kumar, R., Shankar, V., & Jat, M. K. (2015). Evaluation of root water uptake models - A review. In *ISH Journal*
757 *of Hydraulic Engineering* (Vol. 21, Issue 2). <https://doi.org/10.1080/09715010.2014.981955>
- 758 Kuppel, S., Tetzlaff, D., Maneta, M. P., & Soulsby, C. (2018). EcH2O-iso 1.0: Water isotopes and age tracking
759 in a process-based, distributed ecohydrological model. *Geoscientific Model Development*, 11(7), 3045–3069.
760 <https://doi.org/10.5194/gmd-11-3045-2018>
- 761 Landgraf, J., Tetzlaff, D., Birkel, C., Stevenson, J. L., & Soulsby, C. (2023). Assessing land use effects on
762 ecohydrological partitioning in the critical zone through isotope-aided modelling. *Earth Surface Processes*
763 *and Landforms*, 48(15), 3199–3219. <https://doi.org/10.1002/esp.5691>
- 764 Landgraf, J., Tetzlaff, D., Wu, S., Freymüller, J., & Soulsby, C. (2022). Using stable water isotopes to understand
765 ecohydrological partitioning under contrasting land uses in a drought-sensitive rural, lowland catchment.
766 *Hydrological Processes*, 36(12). <https://doi.org/10.1002/hyp.14779>
- 767 Luo, S., Tetzlaff, D., Smith, A., & Soulsby, C. (2024). Assessing impacts of alternative land use strategies on
768 water partitioning, storage and ages in drought-sensitive lowland catchments using tracer-aided
769 ecohydrological modelling. *Hydrological Processes*, 38(4). <https://doi.org/10.1002/hyp.15126>
- 770 Mahmood, R., Pielke, R. A., Hubbard, K. G., Niyogi, D., Dirmeyer, P. A., McAlpine, C., Carleton, A. M., Hale,
771 R., Gameda, S., Beltrán-Przekurat, A., Baker, B., McNider, R., Legates, D. R., Shepherd, M., Du, J., Blanken,
772 P. D., Frauenfeld, O. W., Nair, U. S., & Fall, S. (2014). Land cover changes and their biogeophysical effects
773 on climate. *International Journal of Climatology*, 34(4). <https://doi.org/10.1002/joc.3736>
- 774 Neill, A. J., Birkel, C., Maneta, M. P., Tetzlaff, D., & Soulsby, C. (2021). Structural changes to forests during
775 regeneration affect water flux partitioning, water ages and hydrological connectivity: Insights from tracer-
776 aided ecohydrological modelling. *Hydrology and Earth System Sciences*, 25(9), 4861–4886.
777 <https://doi.org/10.5194/hess-25-4861-2021>
- 778 Orth, R., & Destouni, G. (2018). Drought reduces blue-water fluxes more strongly than green-water fluxes in
779 Europe. *Nature Communications*, 9(1). <https://doi.org/10.1038/s41467-018-06013-7>
- 780 Pielke, R. A., Pitman, A., Niyogi, D., Mahmood, R., McAlpine, C., Hossain, F., Goldewijk, K. K., Nair, U., Betts,
781 R., Fall, S., Reichstein, M., Kabat, P., & de Noblet, N. (2011). Land use/land cover changes and climate:
782 Modeling analysis and observational evidence. In *Wiley Interdisciplinary Reviews: Climate Change* (Vol.
783 2, Issue 6). <https://doi.org/10.1002/wcc.144>



- 784 Quandt, A., Neufeldt, H., & Gorman, K. (2023). Climate change adaptation through agroforestry: opportunities
785 and gaps. In *Current Opinion in Environmental Sustainability* (Vol. 60).
786 <https://doi.org/10.1016/j.cosust.2022.101244>
- 787 Ricci, G. F., De Girolamo, A. M., & Gentile, F. (2020). Modeling the Effect of Different Management Practices
788 for Soil Erosion Control in a Mediterranean Watershed. *Lecture Notes in Civil Engineering*, 67(June), 125–
789 132. https://doi.org/10.1007/978-3-030-39299-4_14
- 790 Rothfuss, Y., & Javaux, M. (2017). Reviews and syntheses: Isotopic approaches to quantify root water uptake: A
791 review and comparison of methods. *Biogeosciences*, 14(8). <https://doi.org/10.5194/bg-14-2199-2017>
- 792 Smith, A., Tetzlaff, D., Gelbrecht, J., Kleine, L., & Soulsby, C. (2020). Riparian wetland rehabilitation and beaver
793 re-colonization impacts on hydrological processes and water quality in a lowland agricultural catchment.
794 *Science of the Total Environment*, 699. <https://doi.org/10.1016/j.scitotenv.2019.134302>
- 795 Smith, A., Tetzlaff, D., Kleine, L., Maneta, M., & Soulsby, C. (2021). Quantifying the effects of land use and
796 model scale on water partitioning and water ages using tracer-aided ecohydrological models. *Hydrology
797 and Earth System Sciences*, 25(4), 2239–2259. <https://doi.org/10.5194/hess-25-2239-2021>
- 798 Sprenger, M., Tetzlaff, D., & Soulsby, C. (2017). Soil water stable isotopes reveal evaporation dynamics at the
799 soil-plant-atmosphere interface of the critical zone. *Hydrology and Earth System Sciences*, 21(7).
800 <https://doi.org/10.5194/hess-21-3839-2017>
- 801 Sterling, S. M., Ducharme, A., & Polcher, J. (2013). The impact of global land-cover change on the terrestrial
802 water cycle. *Nature Climate Change*, 3(4). <https://doi.org/10.1038/nclimate1690>
- 803 Stevenson, J. L., Birkel, C., Comte, J. C., Tetzlaff, D., Marx, C., Neill, A., Maneta, M., Boll, J., & Soulsby, C.
804 (2023). Quantifying heterogeneity in ecohydrological partitioning in urban green spaces through the
805 integration of empirical and modelling approaches. *Environmental Monitoring and Assessment*, 195(4).
806 <https://doi.org/10.1007/s10661-023-11055-6>
- 807 Tague, C. L., & Band, L. E. (2004). RHESSys: Regional Hydro-Ecologic Simulation System—An Object-
808 Oriented Approach to Spatially Distributed Modeling of Carbon, Water, and Nutrient Cycling. *Earth
809 Interactions*, 8(19). [https://doi.org/10.1175/1087-3562\(2004\)8<1:rrhss>2.0.co;2](https://doi.org/10.1175/1087-3562(2004)8<1:rrhss>2.0.co;2)
- 810 te Wierik, S. A., Cammeraat, E. L. H., Gupta, J., & Artzy-Randrup, Y. A. (2021). Reviewing the Impact of Land
811 Use and Land-Use Change on Moisture Recycling and Precipitation Patterns. In *Water Resources Research*
812 (Vol. 57, Issue 7). <https://doi.org/10.1029/2020WR029234>
- 813 Tetzlaff, D., Carey, S. K., McNamara, J. P., Laudon, H., & Soulsby, C. (2017). The essential value of long-term
814 experimental data for hydrology and water management. In *Water Resources Research* (Vol. 53, Issue 4,
815 pp. 2598–2604). Blackwell Publishing Ltd. <https://doi.org/10.1002/2017WR020838>
- 816 Trenberth, K. E. (2011). Changes in precipitation with climate change. *Climate Research*, 47(1–2), 123–138.
817 <https://doi.org/10.3354/cr00953>



- 818 van Huijgevoort, M. H. J., Tetzlaff, D., Sutanudjaja, E. H., & Soulsby, C. (2016). Using high resolution tracer
819 data to constrain water storage, flux and age estimates in a spatially distributed rainfall-runoff model.
820 *Hydrological Processes*, 30(25), 4761–4778. <https://doi.org/10.1002/hyp.10902>
- 821 Wang-Erlandsson, L., Van Der Ent, R. J., Gordon, L. J., & Savenije, H. H. G. (2014). Contrasting roles of
822 interception and transpiration in the hydrological cycle - Part 1: Temporal characteristics over land. *Earth*
823 *System Dynamics*, 5(2). <https://doi.org/10.5194/esd-5-441-2014>
- 824 Wu, S., Tetzlaff, D., Beven, K., & Soulsby, C. (2025). DREAM(LoAX): Simultaneous Calibration and Diagnosis
825 for Tracer-Aided Ecohydrological Models Under the Equifinality Thesis. *Water Resources Research*, 61(3),
826 e2024WR038779. <https://doi.org/https://doi.org/10.1029/2024WR038779>
- 827 Wu, S., Tetzlaff, D., Goldhammer, T., & Soulsby, C. (2021). Hydroclimatic variability and riparian wetland
828 restoration control the hydrology and nutrient fluxes in a lowland agricultural catchment. *Journal of*
829 *Hydrology*, 603. <https://doi.org/10.1016/j.jhydrol.2021.126904>
- 830 Wu, S., Tetzlaff, D., Yang, X., Smith, A., & Soulsby, C. (2023). Integrating Tracers and Soft Data Into Multi-
831 Criteria Calibration: Implications From Distributed Modeling in a Riparian Wetland. *Water Resources*
832 *Research*, 59(11). <https://doi.org/10.1029/2023WR035509>
- 833 Yang, X., Tetzlaff, D., Müller, C., Knöller, K., Borchardt, D., & Soulsby, C. (2023). Upscaling Tracer-Aided
834 Ecohydrological Modeling to Larger Catchments: Implications for Process Representation and
835 Heterogeneity in Landscape Organization. *Water Resources Research*, 59(3).
836 <https://doi.org/10.1029/2022WR033033>
- 837 Ying, Z., Tetzlaff, D., Comte, J.-C., Wu, S., & Soulsby, C. (2025). Storage Dynamics and Groundwater–Surface
838 Water Interactions in a Drought Sensitive Lowland Catchment: Process-Based Modelling as a Learning
839 Tool. *Hydrological Processes*, 39(5), e70141. <https://doi.org/https://doi.org/10.1002/hyp.70141>
- 840 Yuan, X., Wang, Y., Ji, P., Wu, P., Sheffield, J., & Otkin, J. A. (2023). A global transition to flash droughts under
841 climate change. *Science*, 380(6641). <https://doi.org/10.1126/science.abn6301>
- 842 Zhang, L., Dawes, W. R., & Walker, G. R. (2001). Response of mean annual evapotranspiration to vegetation
843 changes at catchment scale. *Water Resources Research*, 37(3). <https://doi.org/10.1029/2000WR900325>
- 844